catalysts

MDPI

Review

Semiconductor Electrode Materials Applied in Photoelectrocatalytic Wastewater Treatment—an Overview

Elzbieta Kusmierek

Institute of General and Ecological Chemistry, Faculty of Chemistry, Lodz University of Technology, Zeromskiego 116 St., 90-924 Lodz, Poland; elzbieta.kusmierek@p.lodz.pl; Tel.: +48-42-631-31-30

Received: 14 March 2020; Accepted: 16 April 2020; Published: 18 April 2020

Abstract: Industrial sources of environmental pollution generate huge amounts of industrial wastewater containing various recalcitrant organic and inorganic pollutants that are hazardous to the environment. On the other hand, industrial wastewater can be regarded as a prospective source of fresh water, energy, and valuable raw materials. Conventional sewage treatment systems are often not efficient enough for the complete degradation of pollutants and they are characterized by high energy consumption. Moreover, the chemical energy that is stored in the wastewater is wasted. A solution to these problems is an application of photoelectrocatalytic treatment methods, especially when they are coupled with energy generation. The paper presents a general overview of the semiconductor materials applied as photoelectrodes in the treatment of various pollutants. The fundamentals of photoelectrocatalytic reactions and the mechanism of pollutants treatment as well as parameters affecting the treatment process are presented. Examples of different semiconductor photoelectrodes that are applied in treatment processes are described in order to present the strengths and weaknesses of the photoelectrocatalytic treatment of industrial wastewater. This overview is an addition to the existing knowledge with a particular focus on the main experimental conditions employed in the photoelectrocatalytic degradation of various pollutants with the application of semiconductor photoelectrodes.

Keywords: semiconductors; photoelectrocatalysis; photoelectrodes; wastewater treatment

1. Introduction

In the XXI century, energy crisis and environmental pollution constitute two main problems in sustainable development, which is defined as the ability of natural systems to supply the natural resources and ecosystems while meeting current human needs, not affecting the ability of the future generations to meet their needs and without deteriorating of the integrity and stability of the natural systems.

Environmental pollution results in serious climate changes and is the most important threat to human population on a global scale nowadays. Thus, it is important to significantly limit the emission of pollutants to the environment. Industrial sources of environmental pollution generate huge amounts of industrial wastewater, which have serious impact on the environment. Although the industrial wastewater contains various recalcitrant organic and inorganic pollutants, it can be regarded as a prospective source of fresh water, energy, and valuable raw materials. Pollutants that are present in wastewater can be treated and simultaneously converted into methane in microbial fuel cells (MFC) [1–8], becoming a potential source of energy. Conventional sewage treatment systems are often not efficient enough for the complete degradation of pollutants present in the industrial wastewater and they are characterized by high energy consumption. On the other hand, the primary energy

is still supplied from fossil fuels. Their combustion leads to the greenhouse effect and dangerous climate changes [9,10]. The pollution of the environment and increasing demand for energy supply has resulted in the development of renewable energy sources. Sunlight seems to be the cleanest and most abundant renewable source of energy, which should be applied in the industrial wastewater treatment [11].

Industrial wastewater usually contains different recalcitrant pollutants and its composition is complex. The wastewater pollutants include textile dyes, pharmaceuticals, pesticides, heavy metals, pulp and paper, surfactants, and other chemicals. Thus, an application of advanced treatment technologies might be required in order to remove or utilize them. Conventional sewage treatment systems are not efficient enough to completely degrade pollutants present in the industrial wastewater. Moreover, the chemical energy stored in the wastewater is wasted [12]. Therefore, it is important to apply clean, environmentally friendly, and efficient wastewater treatment technologies that can totally remove pollutants, recover fresh water and raw materials, and simultaneously recover the chemical energy contained in the wastewater. One of the alternatives to commonly applied wastewater treatment is heterogeneous photocatalysis. However, this technology has some drawbacks. Although many semiconductor photocatalysts are easily photoexcited by UV or VIS irradiation, are stable, and non-toxic, they suffer from low photocatalytic efficiency due to the fast recombination of holes and electron [13–15]. The photocatalytic treatment of wastewater usually does not degrade pollutants completely but results in a decrease of pollutant concentration and formation of intermediated products. The second alternative to the commonly applied wastewater treatment is electrocatalysis, especially electrochemical advanced oxidation processes (EAOPs) that are applied in the case of organic pollutants treatment [16–19]. However, total degradation of organic compounds present in the wastewater often requires so-called "deep electrooxidation" due to the necessity of high voltages application in order to degrade the pollutants to inorganic compounds, such as CO_2, H_2O, N_2, etc., or to simple organic compounds that are easily biodegradable. These methods are characterized by high energy consumption, making the treatment process uneconomical. The photoelectrocatalytic treatment of industrial wastewater should overcome this problem, especially when it is coupled with energy generation. However, the selection of proper electrode materials applied in the photoelectrocatalytic degradation is very important for achieving a decrease in electrical energy consumption. Special attention should be paid to possible photoexcitation of electrode material by visible light (solar irradiation) instead of harmful and more energetic ultraviolet light. Moreover, high long-term stability, mechanical strength, high corrosion resistance, high efficiency of degradation processes, and low costs should characterize electrode materials.

Solar irradiation is regarded as a clean, safe and limitless source of photons. However, the photoexcitation of electrode materials by low energy photons requires the application of special semiconductors or coupled semiconductors or doped semiconductors that are capable of absorbing sunlight in order to degrade organic pollutants present in the industrial wastewater. Thus, three factors should be considered in the selection of semiconductors applied as electrode materials [20]:

(1) absorption of UV and VIS irradiation;
(2) charge-carrier transport within the semiconductor; and,
(3) interfacial charge transfer.

Besides these parameters, the semiconductor should also be characterized by appropriate position of valence and conduction bands related to oxidation and reduction potentials of pollutants, good electrical conductivity and sufficient stability to be applied in treatment processes implemented in practical applications on a large scale. The above-mentioned parameters are important in both wastewater treatment and energy generation.

The aim of this paper is to present a general overview on the semiconductor materials that are applied as photoelectrodes in the photoelectrocatalytic treatment of pollutants present in the industrial wastewater. The fundamentals of photoelectrocatalytic reactions and mechanism of pollutants treatment

as well as parameters affecting the treatment process are presented first. They are followed by examples of various semiconductor materials applied as photoelectrodes in the treatment of different kinds of pollutants in order to prove the advantages of photoelectrocatalytic treatment processes. This overview is an addition to the existing knowledge with a particular focus on the main experimental conditions employed in the photoelectrocatalytic degradation of various pollutants.

2. Mechanism of Photoelectrocatalysis Applied in Wastewater Treatment

Photoelectrocatalytic (PEC) treatment of wastewater is a combination of heterogeneous photocatalysis and electrochemical degradation. This technique is based on the application of a semiconductor material as an electrode, which is irradiated by light with energy equal to or greater than its band gap energy and simultaneously biased by a potential or current. Thus, a description of the photoelectrocatalytic processes should include photocatalytic and electrochemical reactions.

Generally, the semiconductor materials applied in the photoelectrochemical processes can be divided into two groups: photoanodes (n-type) when oxidation reactions take place at the interface and photocathodes (p-type) when the reduction is the main process. The reactions that proceed during the photoelectrocatalytic treatment of pollutants are various and depend on the semiconductor type. The photocatalytic reactions that take place at n-type semiconductors are presented below [21–25].

2.1. n-Type Semiconductor (SC)

$$SC + h\nu \rightarrow SC\left(e^-_{CB} + h^+_{VB}\right) \quad (1)$$

$$SC\left(h^+_{VB}\right) + H_2O \rightarrow SC + H^+ + OH^\bullet \quad (2)$$

$$SC\left(h^+_{VB}\right) + OH^- \rightarrow SC + OH^\bullet \quad (3)$$

$$SC\left(e^-_{CB}\right) + O_2 \rightarrow SC + O_2^{\bullet-} \quad (4)$$

$$O_2^{\bullet-} + H^+ \rightarrow HO_2^\bullet \quad (5)$$

$$2HO_2^\bullet \rightarrow H_2O_2 + O_2 \quad (6)$$

$$H_2O_2 + SC\left(e^-_{CB}\right) \rightarrow SC + OH^\bullet + OH^- \quad (7)$$

where SC denotes semiconductor, hν—photon energy, VB—valence band in SC, CB—conduction band in SC, h^+—hole, and e^-—electron.

Organic pollutants (OP) are degraded in photocatalytic processes according to the reactions [24,25]:

$$OP + OH^\bullet \rightarrow OP^{\bullet-} + H_2O(OH^\bullet) \rightarrow \text{OP degradation products} \quad (8)$$

$$OP + h^+_{VB} \rightarrow OP^{\bullet+} \rightarrow \text{OP oxidation products} \quad (9)$$

$$OP + e^-_{CB} \rightarrow OP^{\bullet-} \rightarrow \text{OP reduction products} \quad (10)$$

If chlorides are present in the solution, then the following photocatalytic reactions are possible [24,26,27]:

$$Cl^- + OH^\bullet \rightarrow Cl^\bullet + OH^- \quad (11)$$

$$Cl^- + h^+ \rightarrow Cl^\bullet \quad (12)$$

$$Cl^\bullet + Cl^- \leftrightarrow Cl_2^{\bullet-} \quad (13)$$

Organic pollutants (OP) photooxidation in the presence of chloride ions proceeds according to the reactions [27–29]:

$$OP + Cl_2^{\bullet-} \rightarrow OP^\bullet + 2Cl^- \quad (14)$$

$$OP^{\bullet+} + O_2 \rightarrow \text{OP oxidation products} + CO_2 \quad (15)$$

Processes, including hydrogen evolution reaction (HER), formation of hydroperoxyl radical and hydrogen peroxide, can be carried out on p-type semiconductor electrodes [25] under UV or VIS irradiation and they are described by the reactions presented below.

2.2. p-Type Semiconductor (SC)

$$SC + h\nu \rightarrow SC\left(e^-_{CB} + h^+_{VB}\right) \quad (16)$$

$$S + e^-_{CB} \rightarrow S^- \quad (17)$$

$$S^- + H^+ \rightarrow S + H^\bullet \quad (18)$$

$$e^-_{CB} + H^+ \rightarrow H^\bullet \quad (19)$$

$$e^-_{CB} + H^+ + H^\bullet \rightarrow H_2 \quad (20)$$

$$S^- + H^+ + H^\bullet \rightarrow H_2 + S \quad (21)$$

$$h^+_{VB} + H^\bullet \rightarrow H^+ \quad (22)$$

$$h^+_{VB} + S^- \rightarrow S \quad (23)$$

$$e^-_{CB} + O_2 + H^+ \rightarrow HO^\bullet_2 \quad (24)$$

$$HO^\bullet_2 + H^+ \rightarrow H_2O_2 + h^+ \quad (25)$$

where S represents a surface state.

The photocatalytic degradation of pollutants often requires the application of UV irradiation instead of VIS light or more accessible solar light [30–32] due to relatively large band gap of semiconductors that were applied in the process. Moreover, the rapid recombination of photogenerated electrons and holes (e^-/h^+) pairs decreases the efficiency of the degradation. The electrochemical degradation of pollutants seems to be an alternative to their photocatalytic degradation, although an application of electrochemical methods also suffers from some limitations.

The electrochemical degradation of pollutants present in the wastewater can proceed directly or indirectly [33–35]. Direct degradation is relatively slow and it requires an application of high voltages or high current densities [36,37], resulting in high energy consumption and high costs. Moreover, it is difficult to achieve the complete degradation of organic pollutants to CO_2, H_2O, N_2, HCl, etc., or to simple organic compounds that are easily biodegradable [36,38]. The electrochemical degradation of pollutants can also proceed indirectly by reactive oxygen species and it is based on the electrogeneration of hydroxyl radicals during oxygen evolution on the anode surface (M) [34,35,39]:

$$M + H_2O \rightarrow M(OH^\bullet) + H^+ + e^- \quad (26)$$

which are converted to oxygen in the following reactions [40]:

$$M(OH^\bullet) + H_2O \rightarrow M + O_2 + 3H^+ + 3e^- \quad (27)$$

$$2M(OH^\bullet) \rightarrow 2M + O_2 + 2H^+ + 2e^- \quad (28)$$

Although $OH^\bullet$ radicals are formed at the electrode surface, their reactivity is limited to about 1μm [41], resulting in significant limitation of oxidation efficiency.

The indirect degradation of pollutants can proceed by in situ electrogenerated chlorine species if chloride ions are present in wastewater. Chlorine electrogenerated at the anode quickly diffuses to

the bulk solution and undergoes the subsequent reactions, resulting in the formation of other species that can degrade pollutants. Subsequently, the following reactions are possible [40,42]:

$$2Cl^- \rightarrow Cl_2 + 2e^- \quad (29)$$

$$Cl_2 + H_2O \rightarrow HClO + Cl^- + H^+ \quad (30)$$

$$HClO^- \leftrightarrow ClO^- + H^+ \quad (31)$$

Moreover, chloride ions can react with photogenerated $OH^\bullet$ radicals forming another radical, according to the reactions [43]:

$$Cl^- + OH^\bullet \leftrightarrow ClOH^{\bullet -} \quad (32)$$

$$ClOH^{\bullet -} + H^+ \leftrightarrow Cl^\bullet + H_2O \quad (33)$$

$$Cl^- + Cl^\bullet \leftrightarrow Cl_2^{\bullet -} \quad (34)$$

In sulphate medium, two other oxidants (peroxodisulphate ions and ozone) can be formed at the anode, according to the following reactions [44,45]:

$$2HSO_4^- \rightarrow S_2O_8^{2-} + 2H^+ + 2e^- \quad (35)$$

$$3H_2O \rightarrow O_3 + 6H^+ + 6e^- \quad (36)$$

Further reaction of peroxodisulphate ions with photogenerated electrons is thermodynamically probable [46]:

$$S_2O_8^{2-} + e_{CB}^- \rightarrow SO_{CB}^{\bullet -} + SO_4^{2-} \quad (37)$$

Sulphate radicals ($SO_4^{\bullet -}$) reveal high reactivity like $OH^\bullet$. Table 1 presents the redox potential of various oxidants and radical species, which can be formed in photochemical and electrochemical processes.

Table 1. Comparison of standard potentials determined for some oxidants and radical species [47–49].

Species	E^0, V (vs. NHE)
$OH^\bullet$	2.80
$SO_4^{\bullet -}$	2.60
$Cl^\bullet$	2.47
O_3	2.07
$S_2O_8^{2-}$	2.01
$Cl_2^{\bullet -}$	2.09
H_2O_2	1.78
$HO_2^\bullet$	1.68
ClO^-	1.49
Cl_2	1.36
O_2	1.23

In the case of electrochemical degradation, it is important to select suitable electrode material, which should be not only stable enough during the process, but should also guarantee the formation of highly reactive radicals and oxidant species, resulting in high efficiency of pollutant treatment.

The efficiency of pollutants treatment achieved in the photocatalytic and electrochemical processes can be enhanced by a combination of these two types of processes. The photoelectrocatalytic degradation of pollutants present in the industrial wastewater has been developed during the last few years due

to the significant development of semiconductor materials applied as photoelectrode materials. The application of external potential or current significantly improves the photocatalytic degradation efficiency, due to the decrease in recombination rate and formation of radicals simultaneously in both (photocatalytic and electrochemical) processes. In the case of photoanodes, the photo-generated electrons are transferred to the external circuit and they are concentrated in the cathode, while photo-generated holes are accumulated in the anode, which guarantees a significant decrease in e^-/h^+ recombination rate [50]. Reactive radicals and highly oxidant species formed both on the cathode and anode can react with pollutants present in wastewater. Figure 1 presents the overall mechanism of photoelectrocatalytic degradation of pollutants.

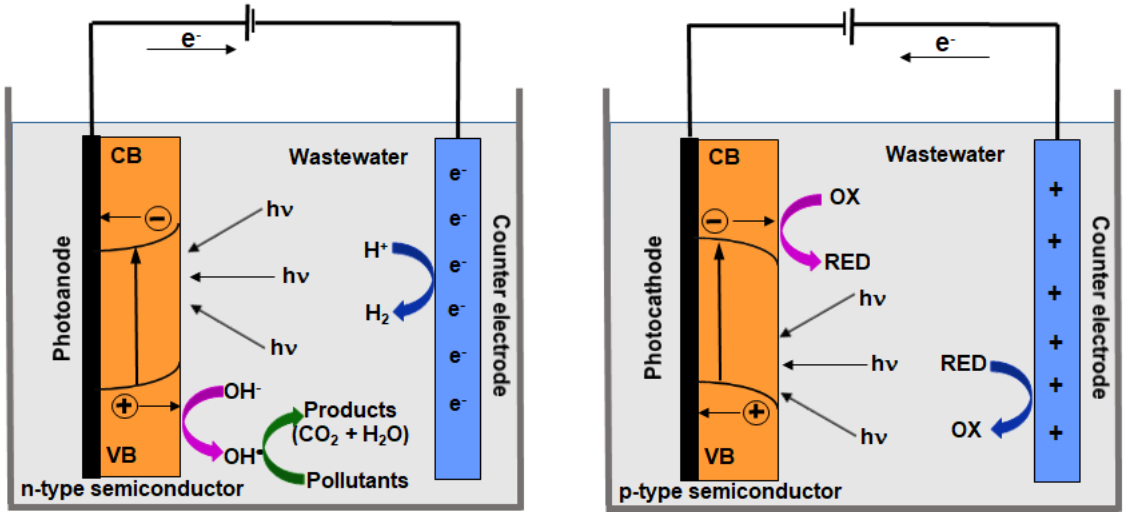

Figure 1. The overall mechanism of photoelectrocatalytic degradation of pollutants in wastewater with the application of n-type and p-type semiconductor electrodes.

The photoelectrochemical reactions in the case of n-type semiconductor applied as working electrode are, as follows [51,52]:

photoanode—irradiation

$$SC + h\nu \rightarrow SC\left(e^-_{CB} + h^+_{VB}\right) \quad (38)$$

anode

$$SC\left(h^+_{VB}\right) + H_2O \rightarrow SC + 1/2O_2 + 2H^+ \quad (39)$$

$$SC\left(h^+_{VB}\right) + H_2O_{ads} \rightarrow SC - OH^{\bullet}_{ads} + H^+ \quad (40)$$

$$SC\left(h^+_{VB}\right) + OH^-_{ads} \rightarrow SC - OH^{\bullet}_{ads} \quad (41)$$

$$SC\left(h^+_{VB}\right) + OP_{ads} \rightarrow SC + OP^{\bullet +}_{ads} \quad (42)$$

cathode

$$H_2O + e^- \rightarrow 1/2H_2 + OH^- \quad (43)$$

Similar reactions proceed while p-type semiconductor is applied as a photocathode:

photocathode—irradiation

$$SC + h\nu \rightarrow SC\left(e^-_{CB} + h^+_{VB}\right) \quad (44)$$

cathode

$$SC\left(e^-_{CB}\right) + O_2 + 2H^+ \rightarrow H_2O_2 + SC\left(h^+_{VB}\right) \quad (45)$$

$$SC\left(e^-_{CB}\right) + H_2O_2 \rightarrow OH^- + OH^{\bullet} \quad (46)$$

$$SC\left(e^-_{CB}\right) + OX \rightarrow SC + RED \quad (47)$$

anode

$$2H_2O \rightarrow O_2 + 4H^+ + 4e^- \quad (48)$$

The photoelectrocatalytic degradation of pollutants present in wastewater takes advantage of heterogeneous photocatalysis with simultaneous electrocatalysis by using a biased potential or current at a photoanode or photocathode. This results in an increase in the pollutant removal efficiency due to the fact that different radicals are formed both in the electrocatalytic and photocatalytic processes simultaneously. The improvement of pollutant removal efficiency in the photoelectrocatalytic process requires the consideration of all parameters influencing both electrochemical and photochemical processes and including the proper selection of a semiconductor material as well as the process parameters. The most important factors influencing efficiency of the photoelectrocatalytic process are, as follows [53]:

photoelectrode type;
light source and its intensity;
pH solution value;
supporting electrolyte—its type and concentration;
counter electrode type;
thickness of semiconductor film on electrode surface;
applied potential or current; and,
design of photoelectrochemical reactor.

Photoelectrode Type

Photoelectrodes applied in photoelectrocatalytic cells consist of a semiconductor supported on a conductive substrate. Semiconductor material must be selected while taking the position of CB and VB into consideration. In the case of water splitting, CB position should be more negative than the potential at which H_2 generation occurs. Similarly, VB position should be more positive than the potential at which O_2 generation is observed [11]. That means relatively wide absorption band, which is undesirable in the case of solar light absorption.

The redox reactions occurring at photoelectrodes can be controlled by the applied potential or current, which means the improvement of reaction selectivity. Moreover, the application of potential or current enables controlling the Fermi level in a semiconductor, resulting in the improvement of charge separation.

The photocatalytic material (semiconductor) should be immobilized at the electrode surface in order to avoid the complicated separation of the photocatalyst applied in the slurry system. In the proper reactor arrangement, the immobilization of the photocatalyst does not decrease its photocatalytic activity [50].

Applied Potential or Current

The photoelectrocatalytic treatment of wastewater requires an application of constant bias potential to a photoelectrode or constant current [53]. Photoreactors are usually equipped with three or two electrode systems, depending on the operation conditions. The potential or current range within which photoelectrocatalytic treatment is performed should be properly selected taking into consideration the efficiency of treatment process and stability of materials applied as electrodes. The treatment efficiency strongly depends on the recombination of e^-/h^+, which can be prevented by external potential or current supplied to photoelectrodes. The external current is even more advantageous due to less complicated reactors with a set of two electrodes instead of three electrodes.

Supporting Electrolyte

The photoelectrochemical treatment of wastewater should be carried out in the presence of a supporting electrolyte. The supporting electrolyte increases the conductivity of a solution that must

guarantee good ion transfer in the treated wastewater. The conductivity also prevents recombination of e^-/h^+ pairs. Moreover, it has significant impact on the applied bias potential or current and the resulting consumption of electrical energy. The type of supporting electrolyte influences the efficiency of the photoelectrocatalytic degradation of pollutants present in wastewater due to formation of different oxidant or reductant species including various radicals with different reactivity [54,55]. The most common electrolytes include NaCl and Na_2SO_4 solutions. In the case of NaCl, active chlorine species and radicals are formed, except for $OH^\bullet$ radicals, and take part in pollutants degradation. In the presence of Na_2SO_4, peroxodisulphate ions and sulphate radicals with comparable reactivity as $OH^\bullet$ radicals can be also generated and take part in the degradation of pollutants. An increase in supporting electrolyte concentration results in the enhancement in pollutants degradation due to formation of higher amounts of reactive species and higher conductivity of the solution [56,57]. On the other hand, the supporting electrolyte affects not only pathway of pollutant degradation, but also the corrosion of photoelectrodes [58].

pH Solution Value

The pH value determined for treated watewater is related to the supporting electrolyte and it is another parameter that is important in photoelectrocatalytic processes. This parameter strongly affects adsorption and dissociation of substrate molecules and distribution of charges on the photocatayst surface and potential of CB and VB [54,55]. Moreover, pH affects the formation of reactive species and radicals. For example, $OH^\bullet$ radicals are regarded as predominant oxidation species at neutral and high pH values, while, at low pH values, the positive holes are considered as the major oxidant species [59]. Generally, the photoelectrocatalytic degradation of organic pollutants proceeds easier at higher pH values due to a higher number of hydroxyl groups, which can be easily oxidized to very reactive $OH^\bullet$ radicals. At low pH values, the reduction of electrons in CB takes part in the degradation of organic pollutants, resulting in reductive cleavage of azo bonds [60]. The pH of wastewater also influences the stability and corrosion of photoelectrodes.

Light Source and Its Intensity

Light intensity has significant impact on the extent of photogenerated e^-/h^+ pairs and the kinetics of photocatalytic reactions due to increasing concentration of reactive radicals [55,61–63]. The higher light intensity causes higher probability of the photocatalysts excitation and the recombined electrons re-excitation. It was reported that, under low light intensities (below 250 W m^{-2}), the photoreaction rate is proportional to the light intensity. If moderate light intensities (higher than 250 W m^{-2}) are applied, then the photoreaction rate is proportional to square root of the light intensity, but, under high light intensities, the photoreaction rate does not depend on the light intensity [64,65]. On the other hand, the higher intensity causes sometimes more energy waste instead of more efficient degradation of pollutants. The energy band structure of a semiconductor plays important role in the utilization of light energy. In heterogeneous systems applied in PEC degradation of wastewater, light energy losses include five reasons [64]:

(1) photons with energy lower than a band gap in a semiconductor do not excite e^-/h^+ pairs and are wasted as a heat;
(2) photons with energy higher than a band gap in a semiconductor are absorbed and the energy equal to E_g is used in e^-/h^+ pair excitation, while the remaining energy is lost as a heat;
(3) some part of a light can be reflected by semiconductor surface and absorbed by the surface of other objects resulting in energy losses;
(4) light transmitted through a semiconductor layer can be absorbed by a support and cause light losses; and,
(5) recombination of e^-/h^+ pairs cause that photons are not utilized effectively and heat is released.

These energy losses can be eliminated by an appropriate wavelength range of light emitted by the lamp, a decrease in the reflection of semiconductor surface, appropriate semiconductor thickness, and light intensity.

Taking into consideration that the light intensity is not uniformly distributed inside the photoreactor [66], it is important to determine the optimum light intensity in order to increase the efficiency of the photoelectrocatalytic degradation and minimize the energy consumption. The distribution of the light inside the photoreactor and, in fact, inside wastewater, depends on lamp-reactor geometry. Three common geometrical configurations of photoreactors are known: annual, elliptical, and parabolic [66]. The annular photoreactor is characterized by the placement of a lamp at the center of the cylindrical vessel. One of the drawback of this geometry is a nonuniform light intensity distribution, depending on a distance inside the reactor which can be overcome by smaller annular region with the thickness lower than 2 cm. Another drawback is related to heat removal which can be also overcome by continuous flow of a solution. In the case of elliptical geometry, a light source is placed at one of ellipse foci and the reactor tube at the other one. However, the surface of the vessel should reflect most of the light that is emitted by the light source. This geometrical configuration is applied when heat must be removed from the lamp and it is also released from highly exothermic reactions. The elliptical reactors are applied in the case of opaque liquids when the reflectivity of container is very important.

Moreover, light sources emitting harmful UV irradiation should be replaced with VIS irradiation or solar light. This requires the proper selection of a semiconductor material that can be excited by light photons with lower energy and can decrease light energy losses.

Counter Electrode

In the case the photoelectrochemical reactor, the counter electrode is a cathode or anode, depending on the working electrode—photoanode or photocathode. The counter electrode plays an important role in the inhibition of recombination between e^- and h^+ by using the external constant potential or current [21,50]. Other factors, like scavengers, should also be considered along with the external bias, since they can reduce recombinations, due to bulk and surface recombinations. However, very fast recombinations with lifetime of picoseconds or nanoseconds are possible, and result in low quantum yield [53].

The role of the counter electrode is still underestimated. Besides the recombination inhibition, this electrode can be useful in the generation of additional oxidant or reductant species, including reactive radicals. In the case of the photoelectrochemical cell with a photoanode and a cathode, the electroreduction of oxygen and the formation of H_2O_2 is possible [34]. Furthermore, this electrode is capable of generating $OH^\bullet$ radicals from H_2O_2 under UV irradiation [35]. This results in an increase in the efficiency of photoelectrocatalytic degradation of organic pollutants in wastewater.

Semiconductor Thickness

The amount of a semiconductor that is immobilized on a substrate related to its thickness has significant influence on the efficiency of the photoelectrocatalytic degradation of pollutants due to the penetration of the light inside the semiconductor film. The semiconductor film should not be too thin because of the insufficient absorption of the light resulting in low efficiency of a photoelectrocatalytic process. Semiconductor film that is too thick can scatter or screen the light and also causes the efficiency of the process to be too low [53]. This is related to dense and compact films of a semiconductor.

Semiconductor film thickness affects light energy conversion and electron transfer. In the case of higher thickness of semiconductor film, relatively high resistance to electron transfer can result in the lower efficiency of the photoelectrodegradation [63].

Reactor Design

The reactor design is a parameter that influences not only the efficiency of photoelectrocatalytic degradation of pollutants present in wastewater, but is also important in the implementation of this

process in industrial application. Parameters affecting the reactor design are similar to those that are mentioned above, i.e. photoelectrode type, supporting electrolyte, pH of wastewater, applied external potential or current, light source, load of organic pollutants, etc. However, additional parameters should be also taken under consideration: temperature, dissolved oxygen, etc. [53]. The immobilized system seems to have more advantages due to the elimination of necessary post treatment of wastewater used in order to remove a photocatalyst. It is important to consider the positioning of the light source versus the solution and photoelectrodes, due to its significant impact on the process efficiency. The simple configuration of the reactor consists of a single chamber, but often with separated compartment for anode and cathode [61]. Flat photoelectrodes allow for maximum light exposure and can be applied in a simple design.

3. Semiconductor Materials Applied in Photoelectrocatalytic Wastewater Treatment

Semiconductor materials are often applied in the photocatalytic treatment of wastewater. However, photocatalysis in wastewater treatment reveals some inconveniences. Photocatalytic treatment can be performed in two modes: suspension and immobilized system [67–70]. The application of suspended semiconductors requires subsequent processes of semiconductor separation and its recycling from the treated wastewater. Both of the processes are time-consuming and increase the treatment cost. Moreover, photocatalyst particle absorbed UV irradiation and its penetration inside wastewater solution is limited [71]. These inconveniences can be overcome by the immobilization of a semiconductor on a proper support [69,71,72]. On the other hand, the immobilization of the semiconductor results in lower surface area of a photocatalyst and a decrease in a reaction rate [67]. Additionally, semiconductor photocatalysts reveal relatively low photocatalytic efficiency due to the recombination of electrons and holes [73].

The above-mentioned inconveniences make the photocatalytic treatment of wastewater difficult to implement in practical applications on a large scale. A solution to these problems seems to be combination of a photocatalytic treatment with electrochemical oxidation. Subsequently, photoactive material, i.e. semiconductor, can be immobilized on a conductive support to which a bias potential or current is supplied [74]. The immobilization of the semiconductor results in a decrease in its losses during the recovery process.

During the photocatalytic processes, the semiconductor is irradiated by light photons with the energy being equal to or higher than its band gap energy. If the photocatalytic process is combined with the electrochemical degradation, photogenerated e^-/h^+ pairs are separated by the bias potential supplied to the semiconductor [22,51,75–77]. Additionally, combination of photocatalytic and electrochemical techniques results in an increase in wastewater treatment due to the generation of highly reactive hydroxyl radicals ($OH^\bullet$). These radicals are generated by the conducting electrode material and simultaneously by the photoactive material that is irradiated by UV or VIS light. Hydroxyl radicals degrade organic pollutants that are present in wastewater with high rate and non-selectively [78–80].

In the case of photoelectrocatalytic treatment of wastewater, it is important to apply the optimum potential supplied to a semiconductor electrode. This potential should be low enough to prevent the destruction of the semiconductor electrode, and to avoid undesired reactions occurring at specified potentials and consuming the electrical charge, e.g., oxygen evolution reaction in the case of an anode. Moreover, the applied potential has a significant effect on the consumption of electrical energy and the costs of the process. On the other hand, lower potential can decrease the electrochemical treatment efficiency [81]. Thus, it is necessary to optimize the applied potential in order to ensure the high stability of the semiconductor electrode and high efficiency of wastewater treatment resulting from the electrochemical process.

One of the methods for improving the efficiency of photoelectrocatalytic wastewater treatment is the application of semiconductors in the form of nanomaterials. Highly ordered nanomaterials, such as nanotubes, nanwires, nanorods, and nanowalls, are characterized by high surface area compensating

the incoveniences that are related to the semiconductor immobilization. Moreover, nanomaterials are characterized by very good electronic transport [51,82,83].

Special attention should be also paid to the development of highly stable semiconductor materials, which could be activated by solar irradiation. This should result in a decrease of photoelectrocatalytic treatment costs.

A semiconductor reveals electrical conductivity between a conductor and insulator. Three regions can be distinguished in its electronic energy structure: the valence band (VB), the conduction band (CB), and the band gap. At absolute zero, a semiconductor is an insulator due to the fact that the VB is completely filled with electrons, while the conduction band is completely empty [84]. Under irradiation, if the light energy is higher than the band gap in the semiconductor, then electrons are transferred from VB to CB and e^-/h^+ pairs are generated. These pairs can recombine with a release of thermal energy or they can be separated and transferred to the semiconductor surface. In the latter case, they take part in oxidation and reduction processes with pollutants being adsorbed at the surface [85]. However, the VB and CB levels should be thermodynamically consistent with the redox potentials of the adsorbates.

The band gap (E_g) is the main parameter characterizing semiconductors applied as a photoelectrode material. This parameter characterizes the electronic structure of semiconductors and the efficiency of photon absorption is related to its value [86]. E_g can be defined in different ways as the fundamental gap, optical gap, electronic gap, and HOMO-LUMO gap. The fundamental gap is defined as the difference in energy between the first electron affinity (EA) and the first ionization potential (IP), according to the equation [87]:

$$E_g(\text{fund}) = EA - IP \tag{49}$$

The optical gap is the energy of transition between the ground state and the first excited state. Its value is close to the value of E_g(fund) and it can be described by the equation [87]:

$$E_g(\text{opt}) = EA - IP - E_b \tag{50}$$

where E_b is the exciton formation energy significantly lower in comparison with E_g(fund).

The band gap can be also defined as a difference between the top of valence band (E_{VB}) and the bottom of the conduction band (E_{CB}), which can be denoted as the HOMO-LUMO band gap or the mono electronic band gap [87]:

$$E_g(\text{mono}) = E_{CB} - E_{VB} \tag{51}$$

In the case of solids, it can be assumed that E_g(fund) is almost equal to E_g(mono).

The band gap position is another important parameter that characterizes semiconductors applied as photoelectrocatalytic material. In the case of a photoanode or photocathode, the positions of the quasi-Fermi levels of the holes (E_{Fh}) and electrons (E_{Fe}) defines the ability of the semiconductor to oxidation or reduction reactions by presenting the chemical potentials of these charge carriers [87–89]. The quasi-Fermi levels can be calculated according to the following equations:

$$E_{Fe} = E_C - k_B \times T \times \ln\left(\frac{N_{eff,C}}{n_e}\right) \tag{52}$$

$$E_{Fh} = E_V - k_B \times T \times \ln\left(\frac{N_{eff,V}}{n_h}\right) \tag{53}$$

where k_B—the Boltzmann constant, T—temperature, $N_{eff,c/v}$—effective density of states in CB or VB, and $n_{e/h}$—the concentration of electrons or holes.

Taking into consideration the order of values determined for effective density of states in CB or VB and typical charge carrier densities [90,91], the quasi-Fermi levels are close to the minimum and maximum energy of CB and VB, respectively. In photoelectrocatalytic investigations, the minimum

and maximum energy of CB and VB is applied in the evaluation of the redox potentials of the semiconductor [87].

Semiconductor materials commonly applied in wastewater treatment, as electrodes can be generally characterized as n-type and p-type. Figure 2 presents energy level diagrams for n-type semiconductors under equilibrium conditions after semiconductor-electrolyte contact, after illumination, and after subsequent bias potential supplied.

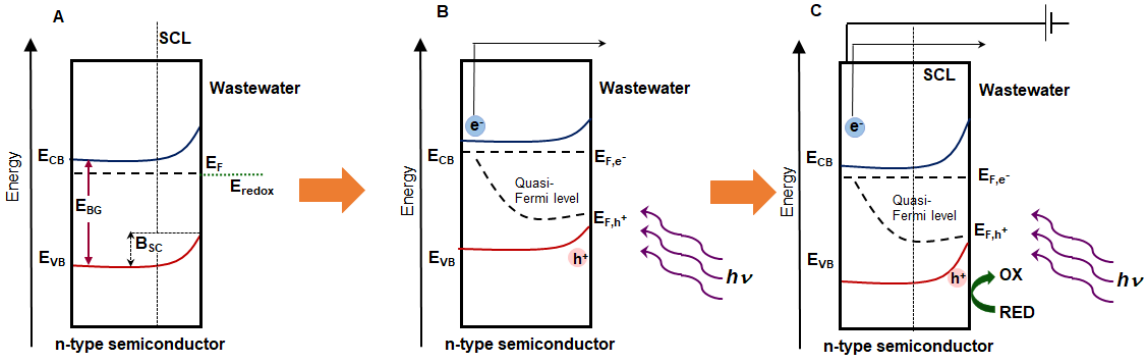

Figure 2. Energy diagram of n-type semiconductor; band positions in a semiconductor under equilibrium condictions, after semiconductor-electrolyte contact (**A**), after irradiation (**B**) and after irradiation and applying a bias potential $E > E_{fb}$ (**C**); E_{fb}—flat band potential, SCL—space charge layer, B_{SC}—band bending in the semiconductor.

In the case of n-type semiconductor, if the position of Fermi level in the redox electrolyte lies below the Fermi level in the semiconductor, and then electrons will be transferred from the semiconductor to the oxidized speces in a solution until the equilibrium is achieved. This leads to the formation of a space charge layer SCL (i.e., depletion layer due to removal of electrons) in the semiconductor and the Fermi levels in both phases must be equal at equilibrium [85]. A bending of bands upward toward the surface takes place. The band bending is equal to the difference between the Fermi levels of the semiconductor and the redox electrolyte [85]. The band bending is defined by the parameter B_{SC} (Figure 2A) and it results in a potential barrier against electron transfer in the n-type semiconductor [88].

Under the irradiation, the semiconductor is photoexcited by the light energy and e^-/h^+ pairs are generated. The Fermi level rises up upon irradiation [88]. Photoexcitation splits the Fermi level of the semiconductor into two quasi-Fermi levels: the quasi-Fermi level of electrons for the CB (E_{F,e^-}) and the quasi-Fermi level of holes for the VB (E_{F,h^+}). The quasi-Fermi level of majority charge carriers remains close to the original Fermi level, while the quasiFermi level of minority charge carriers shifts away from the original Fermi level (Figure 2B).

The application of a bias potential is a method for controlling the Fermi level in the semiconductor, which results in the change in the band bending [51,84,89]. If the applied potential flattens the band edges, then it is called flat band potential E_{fb}. In this case, the potential drops between surface and the bulk of the semiconductor is zero. If the applied potential is higher than E_{fb} ($E > E_{fb}$) then an increase in band bending and SCL occurs [51,82]. The electrons are depleted and holes are enriched at the surface of the semiconductor (Figure 2C). Electrons that have been excited in the conduction band move through external circuit to the counter electrode where redution reactions may occur.

In the case of p-type semiconductor (Figure 3), quite inverse processes proceed. Its Fermi level is located above the VB top. The depletion layer in this type of the semiconductor is characterized by the depletion of the majority of the carriers—holes in this case. The applied potential lower than E_{fb} ($E < E_{fb}$) results in enrichment of the electrons on the semiconductor surface while the wholes are depleted [50]. The reduction reactions are observed on the semiconductor (photocathode) and oxidation reactions proceed on the counter electrode.

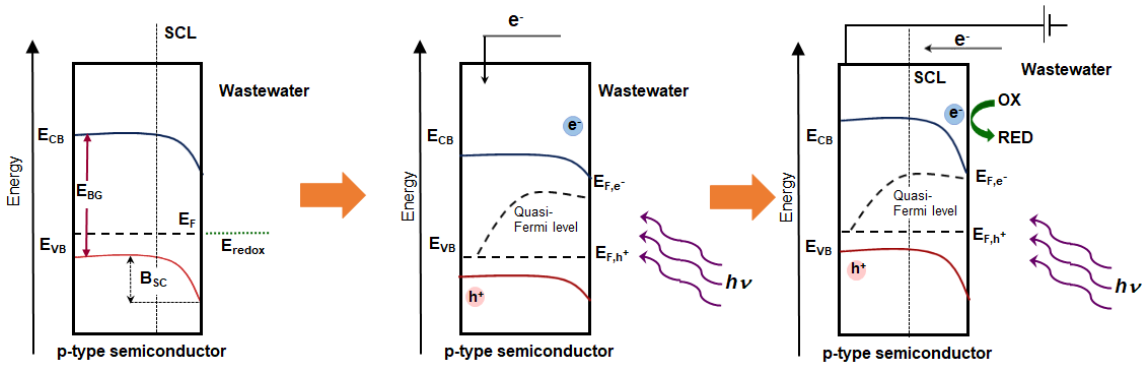

Figure 3. Energy diagram of p-type semiconductor; band positions in a semiconductor under equilibrium conditions, after semiconductor-electrolyte contact (**A**), after irradiation (**B**) and after irradiation and applying a bias potential $E < E_{fb}$ (**C**); E_{fb}—flat band potential, SCL—space charge layer, B_{SC}—band bending in the semiconductor.

The semiconductor materials that are applied in photoelectrocatalytic treatment of wastewater include photoanodes (n-type) and photocathodes (p-type) if oxidation or reduction is the main process at the interface [84]. Thus, photoelectrocatalysis is developed in such wastewater treatment field as:

organic compounds oxidation [92,93];
inorganic ions reduction [94,95];
disinfection [96–98];
metal removal/recovery [99–102]; and,
simultaneous generation of electricity and hydrogen [12,103–105].

The appropriate semiconductor material applied in photoelectrocatalytic wastewater treatment should meet some requirements. The most important requirements are as follows [11]:

wide light absorption spectra range;
suitable band energies;
high charge mobility and long charge carrier diffusion;
high catalytic activity;
high stability; and,
sustainability and low cost.

These requirements are partially fulfilled by single semiconductor materials, composite materials, and doped semiconductors. However, the materials applied as photoelectrodes still need improvement in order to make the implementation of the photoelectrocatalytic treatment of industrial wastewater on a large scale possible.

3.1. Single Semiconductor Photoelectrode Materials

A semiconductor should be immobilized on an appropriate substrate to form a photoelectrode. The substrate plays important role in electron transfer through the semiconductor film. Thus, the substrate should fulfil some criteria: strong adherence, chemical and electrochemical stability, relatively high conductivity, high specific surface area, and strong adsorption affinity towards pollutants [106]. The most common substrates that are applied in supporting semiconductors include silica gel, metals, ceramics, fibres, carbons, graphites, fibres, polymers cellulose, zeolites, glass coated with indium tin oxide or fluorine doped tin oxide glass, etc. [63]. Generally, conductive glasses reveal not enough connection with the semiconductor film (e.g., TiO_2), which results in low transfer efficiency [63,84]. The application of metal supports allows for one to achieve higher photoelectrocatalytic activity of the photoelectrode due to the lower resistance in charge transfer [84].

3.1.1. TiO_2 Photoelectrodes

Titanium dioxide is the most common semiconductor material that is applied in photoelectrocatalytic treatment of wastewater as electrode material, due to its low cost, nontoxicity, and resistance to photocorrosion [107]. TiO_2 occurs in three polymorphs—the stable rutile, metastable anatase, and brookite, showing different properties and band gaps, i.e. 3.0, 3.22, and 3.23 eV, respectively [108,109]. The three polymorphs of TiO_2 were investigated in the photocatalytic degradation of methyl orange (MO) under UV irradiation. During the two-hour experiment, anatase degraded MO in 90%, rutile—60% while brookite—45% [108]. Thus, anatase and rutile forms are mainly applied as photocatalysts. Anatase reveals higher photocatalytic activity than rutile in many cases due to different lattice structure and electronic band structure. The properties of TiO_2 strongly depends on methods of its preparation [110]. In the case of photoelectrodes, TiO_2 can be immobilized on different substrates, e.g., titanium, stainless steel, glass, graphite, etc. The photoelectrodes with TiO_2 as a semiconductor were applied in various photoelectrocatalytic systems for the degradation of organic and inorganic pollutants that are present in wastewater. Table 2 presents an overview of photoelectrodes with TiO_2 applied in degradation of different pollutants under various conditions, over the last two decades.

Table 2. Photoelectrocatalytic degradation of various pollutants with the application of TiO_2 as a semiconductor photoelectrode material.

Semicond./Support	Counter Electrode	Pollutant, Concentration	Light Source Applied Voltage/Current	Supporting Electrolyte	Degradation Efficiency (Process Time)	Other Exp. Conditions—Remarks	Ref.
TiO_2NTs/Ti	Pt/C	MO, 5 mg/L	150 W Xe lamp	0.05 M Na_2SO_4	98% (4 h)	Simultaneous electricity generation	[111]
TiO_2NTs/Ti	Ni	MO, 50 mg/L	UV light (254 nm) 0.75 V	0.01 M Na_2SO_4	MO—100%, COD > 80% (3 h)	-	[112]
TiO_2NTAs/Ti	Pt	MO, 20 mg/L	4 W UV lamp (254 nm) 1.0 mW/cm^2 0.5 V vs. Ag/AgCl	0.01 M Na_2SO_4	80% (3 h)	-	[113]
TiO_2/Ti mesh	RVC (reticulated vitreous carbon)	Orange G, 0.1 mM	8 W mercury lamp (365 nm) 0.68 mW/cm^2 0.71 V vs SCE	0.01 M Na_2SO_4, pH = 6.2	50% (5 h)	-	[114]
TiO_2/Ti	Graphite	Orange G, 0.1 mM	8 W mercury lamp (365 nm) 0.66 mW/m^2 5.5 V	0.1 M Na_2SO_4, pH = 3	54.3% (3 h)	-	[115]
TiO_2/SS mesh	Graphite	Orange G, 64 mg/L	4 W UV lamp (365 nm) 0.33 mW/cm^2 1.0 V vs. SCE	0.01 M Na_2SO_4, pH=3	DOC—38.8% (3 h)	-	[116]
TiO_2NTs/Ti	Graphite	Orange G	UV light (365 nm) 1 mW/cm^2 1 mA	H_2SO_4, pH = 3	60% (3 h)	-	[117]
TiO_2/EG NPs	Pt	MB, 20 mg/L	250 W tungsten-halogen lamp 2.5 V	0.1 M Na_2SO_4, pH = 7	85% (4 h)	-	[118]
TiO_2/PI/Ni	Pt	MB, 0.05 mM	300 W Xe lamp (>430 nm) 0.4 V vs SCE	0.1 M Na_2SO_4	90.2% (1.5 h)	-	[93]
TiO_2/SS NPs	Graphite	Reactive Black 5 (RB), 100 mg/L; KHP, 875 mg/L	UV light	0.14 M Na_2SO_4	RB—77%, KHP —98%, (40 min)	Simultaneous hydrogen generation	[104]

Table 2. *Cont.*

Semicond./Support	Counter Electrode	Pollutant, Concentration	Light Source Applied Voltage/Current	Supporting Electrolyte	Degradation Efficiency (Process Time)	Other Exp. Conditions—Remarks	Ref.
TiO_2/SS	Carbon-PTFE-air-diffusion-electrode	Acid Orange 7 (AO7), 15 mg/L	Sunlight irradiation 1 mA/cm^2	0.05 M Na_2SO_4	AO7—100% (2 h), TOC—40% (4 h)		[119]
TiO_2/Ti	Pt	Direct Black 22 (DB), 20 mg/L	Fluorescent lamp	0.1 M Na_2SO_4	DB–72% (0.4 MPa), COD–58% (0.7 MPa), (2 h)	In the presence of dissolved oxygen at various pressures	[120]
TiO_2/Ti	Steel mesh	Drimaren Red 243X-6BN dye, 25 mg/L	30 W UV lamp (254 nm) 1.5 V	4.2 mM KCl	93% (1 h)	-	[121]
NP-TiO_2/Ti	Pt	Rhodamine B, 5 mg/L	500 W Xe lamp 2 mW/cm^2 0.5 V vs Ag/AgCl	0.1 M phosphate, pH = 7	52.8% (2 h)	-	[122]
TiO_2/FTO	Pt	Phenol, 10 mg/L	4 Leds (3 W) 25 mW/cm^2 1.84 V vs Ag/AgCl	0.1 M Na_2SO_4, pH = 5	73.8% (2 h)	E_{EO} = 599.8 kWh/l	[123]
TiO_2/Ti	Graphite	Phenol, 2 mg/L	3 Xe lamps (solar light) 60 W/m^2 1.0 V vs Ag/AgCl	0.1 M Na_2SO_4, pH = 7.2	88.5% (6h)	EEC =1 kWh/m^3, (50% effic. 115 min)	[124]
TiO_2/Ti mesh	RVC (reticulated vitreous carbon)	2,4,6-trichlorophenol, 10 mg/L	8 W UV-A lamp (365 nm) 2.5 V vs SCE	0.01 M Na_2SO_4	99% (1 h)	with electrogenerated H_2O_2	[125]
TiO_2/Ti NTAs	Pt	Phenol, 20 mg/L	UV Hg-Xe lamp 3.1 mW/cm^2 0.6 V vs Ag/AgCl	0.01 M Na_2SO_4	80% (7 h)	-	[126]
TiO_2/Ti NTs	Pt	2-nitrophenol (2-NPH), 0.1 mM; 4-nitrophenol (4-NPH), 0.1 mM	UV lamp 2 mW/cm^2 0.6 V vs Ag/AgCl	0.5 M NaOH	2-NPH—90%, 4-NPH—95%, (1.5 h)	-	[127]
TiO_2/Ti Blue-TNTs	SS	4-chlorophenol (4-CP), 100 μM	300 W Xe lamp (>320 nm) 1 W/cm^2 1.64 V vs NHE	0.1 M Na_2SO_4	4-CP—100%, TOC—38%, (2 h)	Simultaneous hydrogen generation	[103]

Table 2. *Cont.*

Semicond./Support	Counter Electrode	Pollutant, Concentration	Light Source Applied Voltage/Current	Supporting Electrolyte	Degradation Efficiency (Process Time)	Other Exp. Conditions—Remarks	Ref.
TiO_2/CI (carbon ink)	MnO_2/carbon paper/Ni mesh/Teflon air cathode	Ascorbic acid (AA), 60 μM; Catechol (CAT), 0.5 mM; 2-propanol (IPA), 13.9 mM	60 W tungsten lamp (633 nm, AA) 150 W Xe lamp (IPA, CAT)	0.1 M KCl	AA > 90% (4 h), CAT—25% (3.5 h), IPA—57% (3 h)	Simultaneous electricity generation	[128]
TiO_2/ITO	BDD	Bisphenol-A, 200 μg/L	150 W Xe lamp (>280 nm) 0.32 mA/cm^2	5 mM $HClO_4$, pH = 1	100% (1.5 h)	-	[129]
TiO_2NTs/Ti	Ti	Acetaminophen (Act), 10 mg/L	14 UV lamp (275 nm) 8.0 V	0.02 M Na_2SO_4	Act > 95%, TOC—53%, (5 h)	EEO = 67 kWh/m^3	[130]
TiO_2/EG	Pt	Sulfamethoxazole, 25 mg/L	100 W Xe lamp (AM 1.5G filter) 100 mW/cm^2, 10 mA/cm^2	0.1 M Na_2SO_4 pH = 6.3	COD—60%, (6 h)	-	[131]
TiO_{2-x}/Ti	Graphite	Atrazine (AA), 100 μg/L	Hg lamp (254 nm) 5.4 mW/cm^2, 4 mA/cm^2	0.03 M Na_2SO_4	AA—99.8% (0.5 h), DOC—45.8% (3 h)	-	[132]
TiO_2@TiO_{2-x}/FTO	Pt	MO, 0.1 M	300 W mercury lamp (AM 1.5 G filter) 100 mW/cm^2	0.1 M NaOH	MO—100% (12 min), TOC—72% (20 min)	Simultaneous hydrogen generation	[133]
TiO_2/Ti NTAs	Pt	Tetracycline, 20 mg/L	4 W GE UV lamp 5 mW/cm^2, 2.0 V	0.1 M Na_2SO_4,	96.4% (1 h)	-	[134]
TiO_2/FTO NPs nanoporous	Pt	Tetracycline, 10 mg/L	4 W UV lamp (254 nm) 2.5 mW/cm^2 0.5 V vs Ag/AgCl	0.02 M Na_2SO_4	80% (3 h)	-	[23]
TiO_2/Ti	Vitreous carbon	Chlortetracycline (CTC), 32 μg/L	Hg lamp (254 nm) 6.0 mW/cm^2, 0.39 A	0.5 M Na_2SO_4, pH = 8	CTC—98%, TOC—67%, TN—69%, (2 h)	Simultaneous H_2O_2 generation	[135]
TiO_2/Ti nanorods	Pt	Sulphamethoxazole, 2 mg/L	4 W UV-A lamp 0.5 V vs Ag/AgCl	10 mM Na_2SO_4	100% (70 min)	-	[43]

Table 2. *Cont.*

Semicond./Support	Counter Electrode	Pollutant, Concentration	Light Source Applied Voltage/Current	Supporting Electrolyte	Degradation Efficiency (Process Time)	Other Exp. Conditions—Remarks	Ref.
TiO_2/Ti Nanostructure	Vitreous carbon	Carbamazapine (CBZ), 10 mg/L	Hg lamp (254 nm) 6.9 mW/cm^2, 0.3 A	0.05 M Na_2SO_4	CBZ—73.5%, TOC—21.2%, (2 h)	-	[136]
TiO_2/Ti Nanostructure	Pt	Tamol—anionic surfactant, 0.009% (m/v)	125 W Hg lamp (315–400 nm) 9.23 W/m^2 1.0 V vs Ag/AgCl	0.1 M Na_2SO_4, pH = 2	Tamol—100%, TOC—94%, (1.5 h)	-	[137]
TiO_2NTs/Ti	Ti mesh	Cr (VI), 17.7 mg/L	8 W bacteria lamp (254 nm) 3.1 mW/cm^2 1.5 V	0.5 M citric acid, 1 M NaCl, pH = 2.5	100% (1 h)	-	[138]
TiO_2/ITO NPs	Pt	Ag^+, Pb^{2+}, Cu^{2+}, $Cr_2O_7^{2-}$, 0.2 mM	300 W UV lamp (311 nm) 21.5 W/m^2	05 M NaCl	100% (160 min)	Simultaneous electricity generation	[99]
TiO_2/FTO Nanorods	Pt	U(VI), 0.5 mM	300 W Xe lamp (AM 1.5 G filter) 100 mW/cm^2 0.45 V vs SCE	0.1 M NaCl, ethanol	>99% (12 h)	-	[139]
nano-TiO_2/Ni	MWCNTs air cathode	Pharmaceutical wastewater, COD, 3150 mg/L, Color (units)—825	250 W Hg lamp (≥365 nm) 6.17 mW/cm^2 10 V	0.1 M NaCl, pH = 3	Color—78.5%, COD—93.5%, (2 h)	-	[140]
TiO_2NTs/Ti	PPy/CC Nanostructure	Real textile wastewater COD, 108 mg/L	11 W Hg lamp (254 nm), 3 mW/cm^2	pH = 3	COD—74.1%, (4 h)	Simultaneous electricity generation	[141]

Abbreviations: MO—methyl orange, MB—methylene blue, NTs—nanotubes, NTAs—nanotube arrays, NPs—nanoparticles, FTO—fluorine doped tin oxide glass, ITO—indium tin oxide glass, SS—stainless steel, EG—exfoliated graphite, DOC—dissolved organic carbon, TOC—total organic carbon, TN—total nitrogen, EEC—electrical energy consumption.

Table 2 presents a comparison of results of degradation of various pollutants with the application of TiO_2 as photoelectrode in the photoelectrocatalytic process, as described by several authors. TiO_2 was deposited on various substrates including Ti, W, ITO, FTO, SS, and EG. TiO_2 was also deposited in the form of nanoparticles, nanotubes, nanorods, and in nanocrystalline form, strongly affecting TiO_2 properties, depending on the method of preparation. The application of TiO_2 as a nano material was one of the methods for band gap modification and enabled photoexcitation of photoanodes by visible light. Counter electrodes applied in PEC systems was usually Pt, but also stainless steel, carbon, graphite, or BDD was applied. The counter electrode had significant effect on the PEC efficiency as it was described in [114]. The light sources supplied irradiation from the UV or VIS region with different intensities. Generally, PEC was applied in the degradation of organic compounds, including azo dyes, pharmaceuticals, and pesticides. However, it was also possible to remove metal ions, e.g., Ag(I), Pb(II), Cu(II), Cr(VI), and U(VI). The degradation efficiency was relatively high and significantly higher than in the photocatalytic process without external bias potential or current, or in the electrocatalytic process. However, it should be noted that the degradation efficiency was usually related to a decrease in pollutant concentration or the decolorization of the solution, especially in the case of dyes. This does not indicate solution mineralization and total degradation of pollutants with the formation of inorganic compounds or simple organic compounds that can be easily degraded with the application biological methods. Some authors described also determination of changes in TOC or COD values which can be attributed to the mineralization of pollutants. It is worth noting that a decrease in TOC or COD values were clearly lower in comparison with the degradation efficiency and required higher times of PEC treatment. Moreover, the concentration of the pollutants in all of the described processes was relatively low. Taking into consideration, especially dyes, their possible concentrations in wastewater can be significantly higher, even up to 2 g/L [142], which means higher colouration of wastewater solution and lower penetration of the irradiation, resulting in lower degradation efficiency.

Among TiO_2 photoelectrode materials, a bifunctional electrode draws attention. This electrode was applied in 2-nitrophenol degradation in the PEC process [143]. TiO_2 photocatalyst was coated on one side of the Ti substrate, while Ta_2O_5-$IrO_2$was coated on the other side and it formed electrocatalytic thin film. During a 3 h process, the degradation efficiency of the organic compound achieved the value of 90%. The hydroxyl radicals participating in the organic compound degradation were formed in the photoelectrocatalytic and electrocatalytic processes occurring at both sides of the electrode.

The selection of an effective semiconductor applied as a photoelectrode in wastewater treatment requires the consideration of several factors. These factors include PEC degradation efficiency, semiconductor stability, treatment conditions, regulations, wastewater post-treatment conditions, PEC costs, etc. Among these factors, the costs of the process are very important. They include electrical energy consumption, which constitutes the main part of the operating costs [48,51]. PEC processes of wastewater treatment are regarded as consuming electrical energy and are usually characterized by the consumption of electrical energy per mass E_{EM} (kWh/kg) or electrical energy per order E_{EO} (kWh/m^3/order), as described by the following equations [51,144]:

$$E_{EM} = \frac{P \times t \times 10^6}{V \times (C_0 - C_t)} \quad (54)$$

$$E_{EO} = \frac{P \times t \times 1000}{V \times \lg(M_0/M_t)} \quad (55)$$

where: P—the rated power (kW) of the system, V—volume of treated wastewater (L), t—treatment time (h), C_0 and C_t—initial and final mass concentrations (mg/L), M_0 and Mt—initial and final molar concentrations (mol/L), and V—volume of treated wastewater (L). The electrical energy consumption per order is the electrical energy used in degradation of a pollutant by one order magnitude in unit volume of wastewater. The electrical energy consumption seems to be relatively high in PEC processes, although being lower than in other alternative treatment methods. The EEO values

achieved in the degradation of phenol in photocatalytic process and anodic oxidation were 3732.6 and 8367.7 kWh/L, while photoelectrocatalytic degradation resulted in 599.8 kWh/L [124]. However, the E_{EO} value determined for acetaminophen degradation in the PEC process was only 67 kWh/m^3 [130]. The costs of PEC process can be decreased by the application of semiconductor photoelectrodes activated by solar light.

3.1.2. Other Single Semiconductor Photoelectrode Materials

TiO_2 is not the only semiconductor applied as photoelectrode material. There are several papers describing application of ZnO, Fe_2O_3, SnO_2, CuO/Cu_2O, $BiPO_4$, $BiVO_4$, WO_3, etc., semiconductor photoelectrodes in the degradation of various pollutants that are present in wastewater. These semiconductors are characterized by band gaps that are different than in TiO_2, except for ZnO (Table 3).

Table 3. Band gaps of semiconductors applied as photoelectrodes in the photoelectrocatalytic degradation of various pollutants.

Semiconductor	Band Gap, eV	Ref.
SnO_2	3.8	[107,145]
ZnO	3.2	[84]
WO_3	2.6	[84,107]
CdS	2.25	[107]
Fe_2O_3	2.1–2.2	[84,107]
MoS_2	1.7–1.9	[146]
MoO_3	3.2	[147,148]
Cu_2O	1.95–2.2	[84]
ZrO_2	ca. 5.0	[149]
$BiVO_4$	2.4–2.5	[150,151]
Bi_2MoO_6	2.5–2.8	[152]
Bi_2WO_6	2.82	[153]

ZnO is an n-type semiconductor with similar photocatalytic properties as TiO_2. However, its chemical instability in aqueous solutions is its main drawback related to the following reactions [107]:

$$ZnO + 2H^+ \leftrightarrow Zn^{2+} + H_2O \quad (56)$$

$$ZnO + H_2O \leftrightarrow Zn(OH)_2 \quad (57)$$

This results in limited pH range in which ZnO is stable. Nevertheless, ZnO was investigated as a semiconductor material being applied in photoelectrocatalytic degradation of various pollutants present in wastewater (Table 4).

SnO_2 is also an n-type semiconductor, but with relatively high band gap (3.8 eV) resulting in necessity of UV irradiation application for its photoexcitation. Moreover, the position of CB in SnO_2 makes this semiconductor incapable of reducing oxygen [145]. Thus, this semiconductor has not been applied as photoelectrode material in wastewater treatment However, its coupling with other semiconductor materials has been widely described and it is presented in the next section.

The other semiconductors that are presented in Table 3 reveal lower band gaps and they can be excited by visible irradiation. Especially, WO_3 draws attention due to its high stability in acidic solutions, resistance to photocorrosion, high conductivity, and the possibility of photoexcitation by VIS irradiation or sunlight [107,145]. Thus, this semiconductor seems to be most commonly applied in photodegradation of pollutants present in wastewater, except for TiO_2 (Table 4).

α-Fe_2O_3 (hematite) is a semiconductor with low energy of its band gap (2.1–2.2 eV). Furthermore, this semiconductor is characterized by low costs, nontoxicity, and good chemical stability in most aqueous solutions at pH > 3 [154,155]. α-Fe_2O_3 can be applied in photoelectrocatalytic degradation of pollutants rather than in photocatalytic processes due to its high recombination rate of photoinduced e^-/h^+ pairs. This oxide is also characterized by low conductivity, which can be a drawback in its application as a photoelectrode material. However, this drawback can be eliminated by doping α-Fe_2O_3 with suitable metals.

Bismuth vanadate ($BiVO_4$) is another semiconductor with relatively low energy of a band gap (2.4–2.5 eV), which can be excited by sun light [21]. This oxide is non-toxic, but only stable at almost neutral pH. Although this oxide is characterized by low photon-efficiency and is susceptible to photocorrosion [156], it is often coupled with other semiconductors, e.g., WO_3 [157].

CdS is a semiconductor with higher VB and lower resistance to photocorrosion by photogenerated holes [107]. However, it was not only applied in photoelectrocatalytic degradation of organic compounds, but also in solar cells and optoelectronic devices [158].

Table 4. Photoelectrocatalytic degradation of various pollutants with the application of other single semiconductor photoelectrode materials.

Semicond./Support	Counter Electrode	Pollutant, Concentration	Light Source, Applied Voltage/Current	Supporting Electrolyte	Degradation Efficiency (Process Time)	Other Exp. Conditions—Remarks	Ref.
WO_3/W Nanorods	Pt	Chlorfenvinphos (Cf), 20 ppm	1000 W Xe lamp (420 nm), 100 mW/cm^2, 1 V vs Ag/AgCl	pH = 1	Cf—95%, TOC—65% (6 h)	-	[92]
WO_3/Ti	Pt	Cu^{2+}—500 ppm, Ni^{2+}—500 ppm, MB—10 ppm	150 W Xe lamp (AM 1.5G filter) (UV—4.1%, VIS—54.7%, IR—41.2%), 100 mW/cm^2 0.6 V—Cu^{2+}, 0.8 V—Ni^{2+}	0.5 M NaCl	Cu^{2+}—100%, Ni^{2+}—100%, MB > 70% (10 h)	-	[159]
WO_3/EG NPs	Pt	2-nitrophenol (2-NPH), 20 ppm, Orange II, 30 ppm	100 W Xe lamp, (AM 1.5 G filter) 100 mW/cm^2, 10 A/cm^2	0.1 M Na_2SO_4, pH = 6 (3 h), pH = 5.5 (2 h)	2-NPH—82% and TOC—69% (3 h), Orange II—96% TOC—67% (2 h)	-	[160]
WO_3/FTO Nanoplate arrays	Pd/Au/PM PM—porous metal	Urea, 30 mg/L	350 W Xe lamp (AM 1.5 filter), 100 mW/cm^2, 1.2 V vs SCE	0.05 M Na_2SO_4, 0.05 M NaCl, pH = 5	Urea—100%, TOC—50.9%, TN—99.4% (1 h)	-	[161]
WO_3/W Nanocrystals	Cu_2O/Cu photocathode Nanowires	Phenol (Ph), Rhodamine B (RhB), Congo Red (CR), 20 mg/L	350 W Xe lamp (AM 1.5 filter), 100 mW/cm^2	0.1 M KH_2PO_4, pH = 7	Ph—58%, RhB—66%, CR—73% (5 h)	Simultaneous electricity generation	[162]
WO_3/W Nanoporous	Pt	MO 61.1 µmol/L	500 W Xe lamp (>400 nm), 0.1 W/cm^2, 1.0 V vs SCE	0.1 M NaH_2PO_4, pH = 7	MO—99% (3 h), TOC—81.7% (7 h)	-	[163]
WO_3/Ti Nanosheets	Pt	Atrazine (Atr) 20 mg/L	1000 W Xe lamp (360 nm), 40 mW/cm^2, 1.0 V	0.1 M H_2SO_4	Atr—100% (3 h), TOC—72% (22 h)	-	[164]
α-Fe_2O_3/Ti	Pt	MO, 5 mg/L p-nitrophenol (PNP), 0.05 mM	300 W Tungsten lamp (> 400 nm), $9{\cdot}10^4$ lux, 1.0 V vs SCE	0.1 M Na_2SO_4	MO—79.1 2 (2 h), PNP—46.8%, (4 h)	-	[155]

Table 4. *Cont.*

Semicond./Support	Counter Electrode	Pollutant, Concentration	Light Source, Applied Voltage/Current	Supporting Electrolyte	Degradation Efficiency (Process Time)	Other Exp. Conditions—Remarks	Ref.
Fe_2O_3/FTO	Pt	MB 10 mg/L	Simulated sunlight (AM 1.5G filter), 100 mW/cm^2, 0.2 mA	1.0 M $NaHCO_3$, pH = 2.5	>90% (1 h)	In the presence of 1.0 mM Mn(II)	[165]
MoS_2/ITO Nanosheets	Pt	Ammonia nitrogen (AN), 20 mg/L Bovine Serum Albumine (BSA), 10 mg/L	300 W Xe lamp (> 420 nm), 95.5 mW/cm^2, 0.6 V vs Ag/AgCl	0.1 M Na_2SO_3, pH = 10	AN—80% (6 h) BSA—70% (4 h)	-	[166]
ZnO/FTO	Metal	Textile effluent	UV illumination	-	Color—93%, COD—69% (3 h)	-	[167]
ZnO/EG Nanostructure	Pt	Eosin yellowish dye, $0.1{\cdot}10^{-4}$ M	300 W Quartz tungsten-halogen lamp, UV light filter, 1.0 V	0.1 M Na_2SO_4, pH = 1.5	95% (2 h)	-	[168]
ZrO_2/EG NPs	Pt	Eosin yellowish dye (EY), 20 ppm	250 W quartz tungsten-halogen lamp, 2.5 V	0.1 M Na_2SO_4	EY > 90%, TOC—60% (1 h)	-	[81]
MoO_3/EG Nanorods	Pt	MB, Methyl red (MR), $1{\cdot}10^{-4}$ M	400 W Spectrum solar simulator	0.1 M Na_2SO_4	MB—89%, MR—92% (3 h)	-	[169]
g-C_3N_4	Ti	$Ag(CN)^{2-}$, 0.45 mM	300 W Xe lamp (> 400 nm), 19 mW/cm^2, 1.0 vs SCE	0.05 M Na_2SO_4, pH = 12	Ag—87.7%, CN^-—74.1% (2.5 h)	In the presence of 20 mM H_2O_2	[170]
Bi_2WO_6/CA CA—carbon aerogel	-	Nonylphenol (NP), 1 mg/L	Simulated sunlight, 500 mW/cm^2, 0.6 V vs SCE	pH=10	NP—99.4%, TOC—66.1% (8 h)	with electrosorption	[171]
Bi_2MoO_6/ITO	Ti	$Cu(CN)_3^{2-}$, 250 mg/L	150 W Xe lamp (> 420 nm), 2.0 V vs SCE	1 mM Na_2SO_4, 1 mM NaOH, pH = 11, EDTA/CN = 5:1	CN—99.8%, Cu—91.0% (2 h)	Simultaneous recovery of Cu	[172]

Table 4. *Cont.*

Semicond./Support	Counter Electrode	Pollutant, Concentration	Light Source, Applied Voltage/Current	Supporting Electrolyte	Degradation Efficiency (Process Time)	Other Exp. Conditions—Remarks	Ref.
Bi_2MoO_6/BDD	Pt	Ibuprofen (IB), 10 mg/L, Naproxen (NP), 15 mg/L	150 W Xe lamp (> 420 nm), 2.0 V	0.1 M Na_2SO_4	IB—85% and TOC—76% (2 h), NP—85% and TOC—78% (6 h)	-	[173]
CdS/ITO Nanoparticles	Ti	Bisphenol A, 0.1 mM	Tungsten lamp (400–1100 nm), 0.18 mW/cm^2, 0.8 V vs. Ag/AgCl	0.05 M NaCl	94.1% (20 min)	-	[158]

Abbreviations: MO—methyl orange, MB—methylene blue, NTs—nanotubes, NTAs—nanotube arrays, NPs—nanoparticles, FTO—fluorine doped tin oxide glass, ITO—indium tin oxide glass, SS—stainless steel, EG—exfoliated graphite, DOC—dissolved organic carbon, TOC—total organic carbon, TN—total nitrogen.

Tables 3 and 4 present such semiconductor photoelectrodes as MoS, ZrO_2, MoO_3, Bi_2WO_6, $BiVO_4$, and Bi_2MoO_6, which were applied in the photoelectrocatalytic degradation of various pollutants. Their band gaps are lower than 3 eV, except for ZrO_2 (5.0 eV), MoO_3 (3.2 eV), and SnO_2 (3.8 eV). All of them degraded mainly organic pollutants, including dyes and pharmaceuticals. In the case of MoS, this semiconductor photoelectrode was applied in the degradation of ammonia nitrate under VIS irradiation.

Similarly, as in the case of TiO_2 semiconductor photoelectrodes, the concentrations of pollutants were low and the degradation efficiency was high, but a decrease in COD and TOC was usually lower than decolorization of solutions or decrease in the concentration. Only a few authors also investigated the stability of the photoelectrodes in accelerated stability tests, even though this parameter is very important in wastewater treatment on the large scale.

3.2. Composite Semiconductor Photoelectrode Materials

A combination of two or more semiconductors with appropriately selected band gaps and the energy of CB and VB is a method of improvement of photocatalyst activity [174]. Such combined semiconductors are applied as photoelectrode materials in wastewater treatment. The reason of semiconductor coupling is not only enhancement in utilization of sunlight in photoelectrode excitation, but also the reduction of e^-/h^+ pairs recombination [175,176]. Three combinations of n-type and p-type semiconductors are possible [21]:

(1) p-n heterojunction;
(2) n-n heterojunction; and,
(3) p-p heterojunction.

The p-n heterojunction is characterized by the migration of holes from the p-type to n-type semiconductor and electrons from the n-type to p-type semiconductor due to the fact that electrons are predominant charge carriers in the n-type semiconductors, while holes are the main charge carriers in the p-type semiconductors.

Taking into consideration the position of CB and VB in two coupled semiconductors (A and B), three types of heterojunctions can be distinguished [177,178]:

(1) type I with straddling gap—CB in semiconductor A is higher than CB in semiconductor B, while VB in semiconductor A is lower than VB in semiconductor B;
(2) type II with staggered gap—CB and VB in semiconductor A are higher than CB and VB in the semiconductor B; and,
(3) type III with broken gap.

Figure 4 presents these three types of heterojunctions.

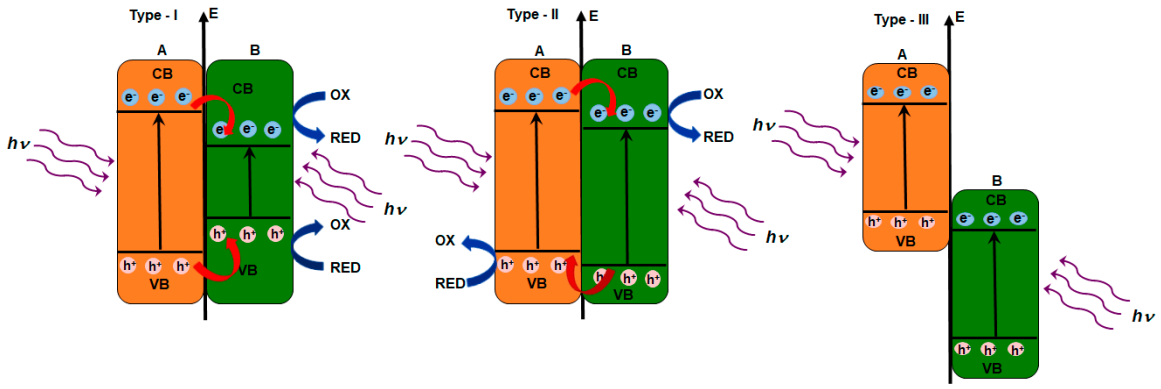

Figure 4. Three types of heterojunction photocatalysts with conduction band (CB) and valence band (VB) position.

In the case of the type I heterojunction, electrons and holes photogenerated in the semiconductor A are transferred to the semiconductor B and the redox reactions take place at the surface of the semiconductor B. Thus, the redox ability of the coupled semiconductors might be lower. The type II heterojunction is characterized by migration of the photogenerated electrons from the semiconductor A to CB in the semiconductor B, while the photogenerated holes migrate in the opposite direction, i.e., from the semiconductor B to VB in the semiconductor A and this is convenient for the separation of e^-/h^+ pairs. In the case of the type III heterojunction, the band gaps of two semiconductor do not overlap and the migration of electrons and holes between two semiconductors does not occur. However, the charge transfer between semiconductors is possible due to broken gap alignment with increasing overall voltage [179,180]. Such heterojunction is unsuitable for the enhancement of photogenerated electrons and holes separation. Photocatalytic activity can be the mostly improved in the case of the type II heterojunction due to the separation of holes and electrons, which makes this heterojunction commonly applied. The coupled semiconductor materials, like SnO_2/TiO_2, $TiO_2/g\text{-}C_3N_4$, or $BiVO_4/WO_3$, are classified as the type II heterojunction, and are applied as photoelectrodes in photoelectrocatalytic degradation of various pollutants that are present in wastewater (Table 5). $Ag/AgCl/g\text{-}C_3N_4$ is a semiconductor material that belongs to type I heterojunctions, while $Ag/AgBr/g\text{-}C_3N_4$ is type II heterojunction [178].

The aforementioned heterojunctions are not the only heterojunctions of semiconductors applied in wastewater treatment as photoelectrodes. The new generation of heterojunctions includes [177]:

(1) p-n heterojunction—coupling of a p-type semiconductor with an n-type semiconductor which results in more efficient separation of photogenerated e^-/h^+ pairs;
(2) surface heterojunction—creation of heterojunction between two crystal facets of a single semiconductor due to their different band structures;
(3) Z-scheme heterojunction, coupling of two different semiconductors and an electron acceptor/donor pair; and,
(4) semiconductor/carbon heterojunction—combination of a semiconductor with carbonaceous nanomaterials, i.e. carbon dots (CDs), carbon nanotubes (CNTs) and graphene.

The semiconductor materials, like $BiOI/CeO_2$, are classified as p-n heterojunction, $g\text{-}C_3N_4\text{-}TiO_2$ as direct Z-scheme heterojunction and $CNT\text{-}TiO_2$ is an example of semiconductor/carbon heterojunction [178].

Table 5. Photoelectrocatalytic degradation of various pollutants with the application of composite semiconductors as photoelectrode materials.

Semicond./Support	Counter Electrode	Pollutant, Concentration	Light Source, Applied Voltage/Current	Supporting Electrolyte	Degradation Efficiency (Process Time)	Other Exp. Conditions—Remarks	Ref.
$TiO_2/WO_3/Ti$	Pt	Reactive Black 5 (RB5), 0.01 mM	125 W Hg lamp, 12.55 mW/cm^2, 1.0 V vs. Ag/AgCl	0.1 M Na_2SO_4, pH = 6	RB5—100%, TOC—85% (2 h)	Simultaneous hydrogen generation	[181]
TiO_2/Cu_2O/FTO	Pt	MO, 20 mg/L	Deuterium lamp, 2 mW/cm^2, 1.5 V vs SCE	0.1 M K_2SO_4, pH = 10	100% 8 h	-	[182]
TiO_2NTs/Bi_2WO_6 Nanosheets	Pt	MO RhB MB Cr(VI)	500 W Xe lamp, solar irradiation simulated, 1.0 V vs Ag/AgCl	0.1 M Na_2SO_4, 0.1 M KCl (Cr(VI))	MO—75.67% (3 h), RhB—66.07% (3 h), MB—95.21% (2 h), Cr(VI)—74.18% (3 h)	-	[183]
TiO_2NTs/Ag-AgBr	Pt	MO RhB MB Cr(VI)	500 W Xe lamp, 1.0 V (MO, RhB, MB) and 0.5 V (Cr(VI)) vs. Ag/AgCl	0.1 M Na_2SO_4	MO—71.97% (3 h), RhB—59.88% (3 h), MB—80.76% (2 h), Cr(VI)—52.24% (3 h)	-	[184]
TiO_2/SnO_2/BDD nanostructure	Pt	Bisphenol A (BPA), 100 mg/L	300 W UV lamp, 20 mA/cm^2	0.1 M Na_2SO_4	BPA—100% (3 h), COD—100% (6 h)	-	[185]
TiO_2NTs/Sb-SNO_2/Ti	Pt	Textile industrial wastewater (TWW-COD = 237 mg/L), Coffee process. wastewater (CWW-COD = 686 mg/L)	UV light (365 nm), 10 mW/cm^2, 30 mA/cm^2	-	TWW-COD—58%, CWW-COD—54% (5 h)	TWW—211.2 kWh/kg COD, CWW—311.2 kWh/kg COD	[186]
CNT-TiO_2/ITO	Pt	Phenol, 20 ppm	300 W UV-free Xe lamp, 1.2 V vs. Ag/AgCl	0.1 M $NaClO_4$, pH = 7	58.3% (2 h)	-	[187]
WO_3/TiO_2/Ti NTs	Pt	Methanol [(M, COD = 5000 ppm)], Formaldehyde (F, 3000 ppm)	Xe lamp (AM 1.5 filter), 100 mW/cm^2, 0.8 V vs Ag/AgCl	0.1 M H_2SO_4	M-COD—35%, F-COD—42% (5 h)	Simultaneous hydrogen generation	[20]

Table 5. *Cont.*

Semicond./Support	Counter Electrode	Pollutant, Concentration	Light Source, Applied Voltage/Current	Supporting Electrolyte	Degradation Efficiency (Process Time)	Other Exp. Conditions—Remarks	Ref.
WO_3/ZnO/FTO NPs	SS	Sugarcane factory wastewater	Sunlight illumination	-	94.44% (100 min)	-	[188]
WO_3/$BiVO_4$/FTO Nanostructure	Ti	Cr(VI), 20 mg/L	150 W Xe lamp, 50 mW/cm^2, 1.7 V	pH = 2.5	100% (40 min)	In the presence of citric acid	[156]
Cu_2O/TNAs/Ti	Pt	Ibuprofen (IB), 10 ppm	100 W Hg lamp, 0.5 V vs Ag/AgCl	-	IB—100% (1.5 h), TOC—49.96% (4 h)	Simultaneous hydrogen generation	[189]
Sn_3O_4/TiO_2/Ti Nanostructure	DSA electrode	Acid yellow 17, 10 mg/L	125 W Hg lamp 9320–400 nm), 72.2 mW/cm^2, 0.5 V vs Ag/AgCl	0.1 M Na_2SO_4, pH = 2	98%, COD—83% (30 min)	-	[190]
SnO_2/PbO_2/Ti	Cu	MO, 50 mg/L	500 W UV light source, 1.5 V vs Ag/AgCl	pH = 2.5	97.4% (40 min)	-	[191]
Sb-doped $Sn_{80\%}$-$W_{20\%}$-O_x/Ti Nanostructure	SS	Phenol red dye, 0.1 mM	10 W UV lamp, 20 mA/cm^2	0.1 M KH_2PO_4	ca. 90% (2 h)	-	[192]
SnO_2/TiO_2NTs	Ti	p-nitrophenol (PNP), 200 mg/L	300 W UV lamp, 20 mA/cm^2	0.1 M Na_2SO_4	PNP—98%, TOC—91% (4 h)	-	[193]
CdTe/ZnO/ITO Nanorods	Pt	Phenol, 100 mg/L	150 W Xe lamp (400 nm), 130 mW/cm^2, 1.0 V vs SCE	0.07 M Na_2SO_4	Phenol—75%, TOC—53.2% (2.5 h)	-	[194]
CdS/TiO_2NTs	Pt	MO, 0.05 mM	300 W Xe lamp (>400 nm), 0.5 V vs SCE	0.05 M K_2SO_4	99.2% (3 h)	-	[195]
CdSe/TiO_2NTAs/Ti	Pt	MO, 10 ppm	300 W Xe lamp (>400 nm), 0.5 V vs SCE	0.2 M Na_2S	85.2% (3 h)	Simultaneous hydrogen generation	[196]

Table 5. *Cont.*

Semicond./Support	Counter Electrode	Pollutant, Concentration	Light Source, Applied Voltage/Current	Supporting Electrolyte	Degradation Efficiency (Process Time)	Other Exp. Conditions—Remarks	Ref.
PbO_2/Co_3O_4NWs/Ti Nanowire arrays	Ti	Reactive Brilliant Blue KN-R dye, 60 mg/L	175 W Xe lamp, 35 mA/cm^2	0.1 M Na_2SO_4	83% (22 h)	-	[197]
AgI/TiO_2NTs/Ti	Ti	Cr(VI), 0.08 mM	Xe lamp (>420 nm), 100 mW/cm^2, 2.0 V vs Ag/AgCl	0.2 M Na_2SO_4	93.6% (70 min)	In the presence of 0.1 M EDTA	[102]
g-C_3N_4/Ag/AgCl/ $BiVO_4$/ITO	Pt	Benzophenone/sewage, 2 ppm	150 W solar simulator (AM 1.5 filter), 1.23 V vs RHE	-	11.15% ($h^{-1}\cdot cm^{-2}$) (2 h)	Simultaneous hydrogen generation	[96]
$Ag_3PO_4/BiVO_4$ Nanostructure	Pt	Norfloxacin, 5 mg/L	300 W Xe lamp (>420 nm), 0.5 V vs SCE	10 mM $NaClO_4$	100% (1.5 h)	-	[198]
Ag/AgCl@chiral TiO_2/FTO	Pt/FTO	Urban wastewater with estrogen (EE2), 0.56 mg/L Cu^{2+}, 1.03 mg/L, TOC—0.56 mg/L, DO—6.7 mg/L, TN—13 mg/L	Solar simulation (AM 1.5G filter)	-	EE2—100%, TOC—100%, Cu^{2+}—100%, TN—70% (2 h)	Simultaneous generation of hydrogen and electricity	[199]

Abbreviations: MO—methyl orange, MB—methylene blue, NTs—nanotubes, NTAs—nanotube arrays, NPs—nanoparticles, FTO—fluorine doped tin oxide glass, ITO—indium tin oxide glass, SS—stainless steel, EG—exfoliated graphite, DOC—dissolved organic carbon, TOC—total organic carbon, TN—total nitrogen.

TiO_2 coupled with WO_3 is a typical example of two n-type semiconductors heterojunction. WO_3 is characterized by lower band gap energy (2.6 eV) in comparison with TiO_2 (3.2 eV). Composite WO_3/TiO_2 nanostructures were applied in the PEC degradation of methanol and formaldehyde [20]. The coupling of these two semiconductors resulted in clearly higher COD reduction in the PEC process in comparison with TiO_2 or WO_3 alone. This was attributed to the improvement of the solar spectrum absorption and, additionally, by the enhancement of the photogenerated carrier transport. The coupling of WO_3 with TiO_2 was also applied in Reactive Black 5 degradation in the PEC process [181]. The bicomponent material applied as a photoanode provided faster dye degradation combined with simultaneous improved hydrogen generation in comparison with the unmodified photoelectrode. CdS is another n-type semiconductor that was coupled with TiO_2 nanotubes and applied as a photoelectrode material in the PEC degradation of methyl orange [195]. Its band gap energy is lower than in TiO_2 and it is equal to 2.4 eV. The coupling of these two semiconductors resulted in a significant increase in the PEC degradation of methyl orange in comparison with unmodified TNTs, under not only UV, but also VIS irradiation. Cu_2O coupled with TiO_2 is an example of p-n heterojunction. Such composite semiconductor was applied in the PEC degradation of methyl orange [182] and ibuprofen [189]. Cu_2O is characterized by the band gap energy that is equal to 2.0–2.2 eV. In the case of methyl orange degradation, its total decolorization was achieved during eight hours of the PEC process if the coupled semiconductor was applied. If the unmodified TiO_2 was applied as photoelectrode material, then total decolorization of the dye solution required 8 h process performed with the application of 1.5 V bias potential. In the case of Cu_2O/TiO_2 photoelectrode, the comparable apparent rate constant of methyl orange degradation was achieved of the bias potential of −0.4 V. It was explained by the improvement in charge separation and extended light absorption spectrum to the visible region. The best degradation efficiency of ibuprofen was achieved at the Cu_2O/TNAs-20 photoelectrode, which revealed the band gap energy of 1.64 eV. The total removal of ibuprofen was observed during the 1.5 h PEC process, while the removal efficiency achieved in photocatalytic process was only 60.4%. Similarly, a decrease in the TOC value was 50% and 30.5% in 4 h PEC process and PC process, respectively. The PEC process was performed with simultaneous hydrogen generation. CdSe is another semiconductor that was coupled with TiO_2 nanotube arrays and applied in the PEC degradation of methyl orange [196]. CdSe is a n-type semiconductor with the band gap energy of 1.7 eV. The composite material revealed high efficiency in methyl orange degradation (PEC process) combined with simultaneous hydrogen generation under visible light irradiation due to the high dispersity of CdSe nanoparticles on outside and inside part of the pore walls of TiO_2NTAs. The AgI/TiO_2-NT composites were applied as photoelectrodes in the PEC removal of Cr(VI) under visible light irradiation [102]. This semiconductor material was characterized by enhanced PEC reduction of Cr(VI) due to the easier generation and separation of e^-/h^+ pairs and reduced charge transfer resistance. The total removal of Cr(VI) was achieved in a 70 min process. TiO_2NTs/Ag-AgBr photoelectrode showed the removal efficiency of methyl orange, rhodamine b, methylene blue and Cr(VI) in the PEC process under visible light irradiation [184]. This photoelectrode properties were attributed to high activity of solar absorption and electron separation in comparison with TiO_2NTs/Ag photoelectrode. g-C_3N_4/Ag/AgCl/$BiVO_4$ heterojunction was applied as the photoelectrode in the PEC degradation of benzophenone sewage with simultaneous hydrogen generation. The application of this photoelectrode resulted in the highest removal efficiency in comparison with other photoelectrodes such as g-C_3N_4/$BiVO_4$, g-C_3N_4, Ag/AgCl/$BiVO_4$, and $BiVO_4$. This was explained by more efficient transport of electrons towards the cathode and reduced recombination rate of the charge carriers, which resulted in the formation of high energetic reactive species, like hydroxyl radicals.

TiO_2 is most commonly applied among the coupled semiconductors. However, the coupled semiconductors without TiO_2 are also applied as photoelectrodes in the degradation of various pollutants. For example, WO_3 was coupled with ZnO and $BiVO_4$ while ZnO was coupled with CdTe. The application of WO_3/ZnO photoelectrode in the PEC treatment of sugarcane factory wastewater under sunlight irradiation [188] seems to be especially interesting. The wastewater degradation

with 99.4% efficiency was achieved in a 1.7 h PEC process. The photostability and reusability of the photoelectrode was investigated and resulted in the conclusion that this photoelectrode was stable and did not undergo photocorrosion. $BiVO_4$ with the monoclinic structure is a semiconductor with a band gap energy of 2.4 eV, which makes it favourable to couple with WO_3. WO_3/$BiVO_4$ was applied as a photoelectrode in Cr(VI) removal [156]. The CB in the coupled semiconductors was more positive than in the pure WO_3 photoelectrode and it resulted in higher reduction ability of photoexcited electrons. Moreover, the heterojunction structure broadened light absorbance range and revealed higher photocurrents due to more efficient e^-/h^+ separation.

The enhanced efficiency of the PEC degradation of norfloxacin was observed in the case of Ag_3PO_4-modified $BiVO_4$ photoelectrode [198]. The band gap that was determined for Ag_3PO_4, $BiVO_4$, and Ag_3PO_4/$BiVO_4$ film was equal to 2.42, 2.54, and 2.51 eV. The enhanced photoelectrocatalytic activity of the tested photoelectrode under visible light irradiation and at low bias potential (0.5 V) was attributed to a better separation of the photogenerated e^-/h^+ pairs. The degradation efficiency increased with higher bias potential and lower norfloxacin concentration due to the contribution of hydroxyl radicals and holes in the oxidation of the organic compound.

CdTe is a semiconductor with the narrow band gap (1.5 eV) that is suitable to absorb solar light. CdTe-ZnO composite nanorods were applied in the PEC degradation of phenol under visible light irradiation [194]. Approximately 75% degradation of phenol was achieved at CdTe-ZnO photoelectrode while the application of ZnO nanorods in the PEC process resulted in 40% degradation. Furthermore, the PC and EC degradation of phenol with the application of CdTe-ZnO composite nanorods resulted in comparable (about 20%) and much lower efficiency than in the case of the PEC process that was performed under visible light irradiation.

Co_3O_4 is a promising photoelectrode material due to its high stability, low cost, and narrow bandgap of 2.07 eV. The compoites of PbO_2 with Co_3O_4 nanowire arrays presented higher PEC activity in the degradation of Reactive Brilliant Blue dye in comparison to Co_3O_4 nanowires, which was attributed to lower charge transfer resistance, larger electroactive surface area and higher ability for the generation of hydroxyl radicals [197].

SnO_2 is another n-type semiconductor worth mentioning due to its application in different composite photoelectrode materials succesfully applied in the PEC degradation of organic pollutants, i.e. p-nitrophenol [193], methyl orange [191], and bisphenol A [185]. TiO_2-NTs/Sb-SnO_2 was the photoelectrode material that was applied in the PEC treatment of textile industrial wastewater and coffee processing wastewater [186]. The decrease in COD value for both types of wastewater was higher than 50% under UV irradiation. The energy consumption was calculated to be 211.2 kWh/kg COD (textile wastewater) and 311.2 kWh/kg COD (coffee processing wastewater). The high service life and reusability of the tested photoelectrode suggested its potential application for the treatment of industrial wastewater on a large scale.

3.3. Doped and Metal-Deposited Semiconductor Photoelectrode Materials

The doping of semiconductors is applied in order to enhance their photocatalytic activity and make their photoexcitation with visible light irradiation possible. Thus, doping is related to band gap engineering. Furthermore, doping can enhance electrical conductivity of a single semiconductor. This is especially important in the case of TiO_2, which is characterized by high electrical resistance at room temperature, resulting in a low rate of electron transfer [52]. If both disadvantages, e.g., low photocatalytic activity and low electrical conductivity, are overcome, then it is possible to minimize the costs of the photoelectrocatalytic treatment of pollutants that are present in wastewater. The semiconductor properties can be modified by doping with [200]:

(1) alkali metals: Li, Mg, Ca;
(2) anions (nonmetal dopants): C, N, F, S, B, I;
(3) different metalloids: B, Si, Ge, Sb;
(4) transition metals: Sc, V, Cr, Mn, Fe, Co, Ni, Cu, Zn, Y, Zr, Nb, Mo, Ag, Ta;

(5) post-transition metals: Al, Ga, In, Sn; and,
(6) lanthanides: La, Ce, Nd, Sm, Eu.

Moreover, a semiconductor can be co-doped or tri-doped with two or even three dopants. Doping results in the replacement of oxygen with the dopant in the crystal lattice.

Photocatalytic activity of semiconductor materials applied as photoanodes can also be enhanced by combining with noble metals (Au, Ag, Pt, and Pd) on a nanometer scale. This is related to different Fermi levels in the semiconductor and noble metal dopant, being characterized by the work function of the dopant and band structure of the semiconductor. Doping results in the formation of Schottky barrier in the doped material [84,107]. Subsequently, the noble metal acts as an electron trap and promotes the interfacial electron transfer from CB of the semiconductor into the metal nanoparticles and recombination of photogenerated e^-/h^+ pairs is reduced. Metal semiconductor materials, such as Ag/TiO_2, Pt/TiO_2, and Au/TiO_2, are synthetized by photodeposition from metal precursors ($AgNO_3$, $HAuCl_4$, or H_2PtCl_6) dissolved in the solution [201].

The deposition of metals on a semiconductor surface is another way to enhance the photocatalytic activity of a semiconductor material [107]. The metal deposition can be performed with an application of electrochemical reduction [202] or dip coating method, followed by a photoassisted reduction of metal ions in aqueous solution under UV irradiation [107,203]. This modification of semiconductor surface is also called "decoration". ZnO that is decorated with Ag nanoparticles is an example of the semiconductor material with enhanced photocatalytic activity [204–206].

Doped and metal-deposited semiconductors were successfully applied as photoelectrode materials in the photoelectrocatalytic degradation of different pollutants that are present in wastewater (Table 6).

Table 6. Photoelectrocatalytic degradation of various pollutants with the application of doped and metal-deposited semiconductors as photoelectrode materials.

Semicond./Support	Counter Electrode	Pollutant, Concentration	Light Source, Applied Voltage/Current	Supporting Electrolyte	Degradation Efficiency (Process Time)	Other Exp. Conditions—Remarks	Ref.
Pt-TiO_2NTs/Ti	Pt	Acid Red 29 (AR29), 85.4 mg/L	125 W Hg lamp, 9.2 W/m^2, 2.0 V vs Ag/AgCl	0.1 M Na_2SO_4, pH = 3	AR29—100%, TOC—92% (2 h)	-	[202]
Pt-TiO_2/ITO	Pt	Formic acid, 15 mM, COD = 239 mg/L	500 W UV lamp, 3.12 mW/cm^2, 1.0 V vs Ag/AgCl	pH = 2.73	COD > 95% (1 h)	-	[203]
Ti^{3+}-TiO_2/Ti	Pt	Rhodamine B (RhB), 0.01 mM, Phenol, 10 mg/L	60 W lamp (>450 nm), 86610 lux, 0.6 V vs SCE	0.1 M Na_2SO_4	RhB—72% (3 h), Phenol—68% (5 h)	-	[207]
N-TiO_2/Ti	Vitreous carbon	Chlortetracycline (CTC), 0.1 mg/L	150 W Xenon lamp (AM 1.5 filter), 6.9 mW/cm^2, 0.6 A	0.07 M Na_2SO_4	CTC—99.6%, TOC—92.5%, TN—90.3% (3 h)	-	[208]
N-TiO_2/ graphene/Ti	Pt	Diazinon, 9 mg/L	36 W Visible light lamps, 0.9 V vs SCE	0.042 M Na_2SO_4, pH = 6	80% (3 h)	Process with electrosorption	[209]
N-TNTs/Ti	Pt	MB, 80 mg/L, RhB, 80 mg/L, BPA, 50 mg/L	300 W tungsten lamp (>420 nm), 213 μW/cm^2, 2 V	0.1 M Na_2SO_4	MB—65.3%, RhB—44.7%, BPA—34.3% (80 min)	-	[210]
Au/TiO_2NTs/Ti	Ti	MO, 5 mg/L	450 W Xe lamp, 0.5 V vs. SCE	0.5 M Na_2SO_4, pH = 7	54.5% (6 h)	-	[211]
N-S-TiO_2NCs/ TNTAs	Pt	MB, 5 mg/L	35 W Xe lamp, 0.4 V vs SCE	0.1 M Na_2SO_4	93.9% (2 h)	-	[212]
N-C-TNTAs/Ti	Pt	Perfluorooctanoic acid, 40 mg/L	100 W Hg lamp, 3.12 mW/cm^2, 1.0 V vs Ag/AgCl	pH = 4	56.1% (3 h)	Simultaneous hydrogen generation	[213]
La-N-TiO_2/Ni	Carbon stick	Malachite green, 30 mg/L	50 W tungsten lamp, 80.4 mW/cm^2, 4 V vs SCE	0.5 M Na_2SO_4	>80% (4 h)	-	[214]

Table 6. *Cont.*

Semicond./Support	Counter Electrode	Pollutant, Concentration	Light Source, Applied Voltage/Current	Supporting Electrolyte	Degradation Efficiency (Process Time)	Other Exp. Conditions—Remarks	Ref.
B-TiO_2NTs/Ti	Ti/Ru	Acid yellow 1 (AY1), 100 ppm	125 Hg lamp, 1.2 v vs Ag/AgCl	0.01 M Na_2SO_4	AY1—100%, TOC—95% (2 h)	-	[215]
TiO_2NBs/AuNPs/Ti	Pt	Tetrabromobisphenol A, 5 mg/L	35 W Xe lamp (>400 nm), 1.5 V vs SCE	0.1 M Na_2SO_4	95% (100 min)	-	[216]
TiO_2NTs/Ag@Au/Ti	Pt	MO Cr(VI)	500 W Xe lamp (AM 1.5 filter), 1.0 V (MO), 0.5 V (Cr(VI))	MO—0.1 M K_2SO_4, Cr(VI)—0.1 M NaCl	MO—98%, Cr(VI)—70% (2 h)	-	[217]
Cu/N-TiO_2/Ti	Graphite	Landfill leachate, COD—186.68 mg/L	50 W tungsten lamp, 80.1 mW/cm^2, 20 V	pH = 2	76.9% (2.5 h)	-	[59]
Cu/TiO_2NTs/Ti	Pt	Rhodamine B (RhB), Cr(VI)	500 W Xe lamp (>400 nm), 0.5 V (RhB), 1.0 V (Cr(VI))	0.1M K_2SO_4, 0.1M KCl	RhB—95.7%(2 h), Cr(VI) —50.7% (2.5 h)	-	[218]
F-PbO_2/Ti	Ti	Reactive brilliant blue KN-R (RB), 60 mg/L	150 W Xe lamp, 35 mA/cm^2	0.1 M Na_2SO_4	RB > 80%, TOC—14.2% (2.5 h)	-	[219]
Ag-ZrO_2/EG	Pt	MB, 20 mg/L	250 W solar symulator, 2 V	0.1M Na_2SO_4, pH = 11	93% (4 h)	-	[37]
Cu-WO_3/FTO	Pt	Bisphenol A (BPA), 60 ppm	150 W vapour metallic lamp, 10 mA/cm^2	0.5 M Na_2SO_4, pH = 8	BPA—ca. 80%, TOC—75% (8 h)	EEC = 11.73 kWh/kg	[220]
$Y_{0.05}Bi_{0.95}VO_4$/FTO	Pt	Rhodamine B, 0.2 mg/L	300 W Xe lamp (>420 nm), 100 mW/cm^2, 0.7 V vs. Ag/AgCl	0.5 M Na_2SO_4	24% (3 h)	-	[221]

Abbreviations: MO—methyl orange, MB—methylene blue, NTs—nanotubes, NTAs—nanotube arrays, NPs—nanoparticles, NBs—nanobelts, FTO—fluorine doped tin oxide glass, ITO—indium tin oxide glass, SS—stainless steel, EG—exfoliated graphite, DOC—dissolved organic carbon, TOC—total organic carbon, TN—total nitrogen, EEC—electrical energy consumption.

Pt decorated TiO_2 nanotubes were applied as photoanodes in the photoelectrocatalytic (PEC) degradation of Acid Red 29 dye [202]. The decoration with Pt resulted in a decrease of TiO_2NT band gap from 3.21 to 2.87 eV. Simultaneously, the decrease in TOC value was 92% in the case of the doped photoelectrode during a 2 h process, while only 66% decrease in TOC was achieved in the same time at the undoped photoelectrode. The improvement of the degradation process was attributed to a better separation of e^-/h^+ pairs, and the generation of additional $OH^\bullet$ radicals due to higher photocatalytic activity of the doped photoelectrode. The degradation efficiency of formic acid was clearly higher in its PEC degradation with the application of Pt deposited TiO_2 photoelectrode [203] and was dependent on the amount of Pt deposited. COD removal efficiencies were higher (>95%) than in the case the photocatalytic process (PC) or PEC process with the application of the undecorated photoelectrode. Additionally, the rates for the PC oxidation or PEC oxidation on Pt-TiO_2 photoelectrode were more than 4 and 5.4 times higher than in the case of the PC oxidation on the undecorated electrode. The deposition of Au at TiO_2 nanotubes resulted in enhanced absorption of visible light and higher activity of PEC degradation of methylene blue under solar light irradiation [211], due to the facilitation of the charge separation and transfer. Doped TiO_2 nanobelts with Au nanoparticles were found to be efficient photoelectrode material in the PEC degradation of tetrabromobisphenol A [216]. The modification of the photoelectrode with AuNPs facilitated the direct utilization of the photogenerated holes in the PEC degradation of the pollutant. TiO_2 nanotubes that were decorated with Ag@Au nanoparticles were applied as photoelectrodes in the PEC degradation of methyl orange and the removal of Cr(VI) [217]. Bimetallic Ag-Au nanoparticles showed a remarkable influence on solar response and PEC activity ofTiO_2NTs, which was attributed to the plasmon mediated electron transfer from Au to Ag sites within core-shell structures. The PEC efficiency of methylene blue and Cr(VI) removal was significantly higher in the case of TiO_2NTs/Ag@Au photoelectrode in comparison with TiO_2NTs and TiO_2NTs/Ag photoelectrodes, and achieved the value of 98% (MO) and 70% (Cr(VI)) during a 2 h process. N doped TiO_2 photoelectrode was applied in the PEC degradation of chlortetracycline [208]. Doping with N resulted in a band gap decrease from 3.2 to 2.3 eV in the case of the photoelectrode that was doped with 3.4 at. % N. This significantly improved a decrease in the pollutant concentration and in TOC, in comparison with the undoped photoelectrode and with the photoelectrodes that were doped with lower amounts of nitrogen. TiO_2 nanotubes doped with N revealed a decrease in a band gap from 3.07 eV (TNTs) to 2.77 eV for N-10-TNTs photoelectrode with the optimum amount of N [210]. This photoelectrode was applied in the PEC degradation of methylene blue, rhodamine B, and bisphenol A with the degradation efficiency of 65.3, 44.7, and 34.3%, respectively, under visible light. The enhanced activity of the photoelectrode material was attributed to the reduction of the transfer resistance of the photoelectrons. N and S co-doped TiO_2 nano-crystallites (NCs) decorated TiO_2 nano-tube arrays (N-S-TiO_2NCs/TNTAs) photoelectrodes revealed a decrease in the band gap from 3.2 (TNTAs) to 2.25 eV [212]. The degradation of methylene proceeded on this photoelectrode with the removal efficiency of 94%, while, in the photocatalytic process, the efficiency was only 58% under the same conditions. The enhancement in the PEC efficiency of the pollutant degradation was attributed to the enhancement of the light absorption in the visible region and the improvement of the transfer and separation of photoinduced charge carriers. C and N co-doped TiO_2 nanotube arrays (C-N-TNTAs) were applied as photoelectrodes in hydrogen generation combined with the simultaneous PEC degradation of perfluorooctanoic acid [213]. Doping with C and N resulted in a band gap decrease from 3.2 eV (TNTAs) to 2.9 eV. The PEC process was the most efficient in the case of the pollutant degradation (56%) in comparison with the PC process (18%) and EC process (5%). Another TiO_2 semiconductor material that was co-doped with La and N was applied in malachite green dye degradation [214]. Doping resulted in a narrowing of the band gap to 2.79 eV and an increase in photocatalytic activity under visible light irradiation in comparison with the undoped TiO_2, which was attributed to the prevention of the phase transition between anatase and rutile phase, and to slow the recombination rate of the photogenerated e^-/h^+ pairs. The co-doped photoelectrode presented higher PEC activity in the degradation of the dye under VIS irradiation, but under relatively high bias voltage of 4 V. TiO_2

self-doped with Ti^{3+} was obtained by the electrochemical reduction method [207] and applied in the PEC degradation of Rhodamine B and phenol. The enhancement of the photoelectrocatalytic responses for the self-doped photoelectrodes in UV and visible region was proved. The doped photoelectrode generated hydroxyl radicals under visible irradiation and revealed higher efficiency in the PEC degradation of the tested pollutants in comparison with the undoped photoelectrode. The doping of TiO_2 nanotubes with boron (B-TiO_2NTs) resulted in a band gap decrease to 2.22 eV [215]. The boron-doped photoelectrode was successfully applied in Acid Yellow 1 dye degradation performed in the PEC process with the rate two times higher than in the PC process under solar irradiation.

TiO_2 is a semiconductor that is most commonly modified by doping and applied as a photoelectrode material. Nonetheless, there are also other doped semiconductors that are applied in the photoelectrocatalytic treatment of different pollutants. Cu doped WO_3 was applied as a photoelectrode in the PEC degradation of bisphenol A [220]. Doping with Cu did not result in a significant change in the band gap of the modified semiconductor, because its value for 1% Cu was 2.96 eV, while WO_3 presented relatively wide band gap energy of 2.6–3.0 eV. Doping with 1% Cu was most beneficial when taking into consideration the removal of the pollutant. The Ag doped ZrO_2/EG semiconductor material presented a band gap of 5.16 eV, i.e. lower than in the case of ZrO_2/EG (5.42 eV) and was applied as photoelectrode in the degradation of methylene blue under solar light [37]. Although this semiconductor material presented minimal degradation efficiency in photocatalytic degradation, the PEC process resulted in a significant degradation of MB, which was attributed to the synergistic effects of Ag and EG (exfoliated graphite). $BiVO_4$ semiconductor doped with Y was applied in the degradation of Rhodamine B dye [221]. Doping with Y resulted in a very slight change in band gap energy. $BiVO_4$ revealed a band gap of 2.5 eV, while the most advantageous modified semiconductor ($Y_{0.05}Bi_{0.95}VO_4$) was characterized by the band gap of 2.52 eV. Photocatalytic degradation of the dye in the presence of the tested photoelectrode was characterized by the degradation efficiency of 18%, while this value increased to 24% in the PEC process. The authors attributed the increase in the degradation efficiency to the applied bias potential, which could promote the separation and transfer of photogenerated holes and electrons in $Y_{0.05}Bi_{0.95}VO_4$ thin film electrode.

The degradation efficiency of different pollutants that were achieved in the photolectrocatalytic process applied with doped semiconductor materials as photoelectrodes was relatively high in most examples presented in Table 6. The mineralization of the pollutant solutions expressed as a decrease in COD or TOC was also high. However, it required a relatively long duration of the PEC process. Only in a few cases, electrical energy consumption was calculated, and the results of accelerated stability tests were presented.

4. Conclusions and Future Perspectives

An overview of semiconductor electrode materials applied in photoelectrocatalytic treatment of various pollutants, including organic compounds, inorganic compounds and metals, was presented. Photoelectrocatalytic reactions and parameters affecting the treatment process were described. Examples of various semiconductor materials with main experimental conditions and results of the pollutants degradation were included in the presentation of strengths and weaknesses of the photoelectrocatalytic process. Undoubtedly, the photoelectrocatalytic degradation of pollutants present in industrial wastewater is a very promising technique in wastewater treatment with potential application on a large scale. In many cases, the photoelectrocatalytic processes are characterized by higher efficiency in comparison with the photocatalytic and electrocatalytic processes, because the applied bias potential or current can significantly facilitate the transfer of photocarriers and simultaneously hinder the recombination of photogenerated electrons and holes. The advantage of the PEC treatment processes results from the synergetic effect of UV or VIS irradiation and external electrical field. Nonetheless, the selection of a proper method for wastewater treatment requires the consideration of not only efficiency of pollutant removal, but also the mineralization degree of wastewater, with possible products formed during pollutant degradation, recovery of water and

raw materials, energy consumption connected with process costs, etc. The PEC processes with the application of semiconductors as photoelectrode materials have many advantages since they are environmentally friendly—no toxic chemicals are required in the treatment, they are easy to operate, and safe due to the ambient conditions of wastewater treatment, sustainable (possible application of sunlight), and cost effective if an appropriate semiconductor material is applied. Thus, the semiconductor materials should still be improved, and some key points should be taken into consideration. First of all, the semiconductor material should be excited by the sunlight, which is commonly available, and the photon absorption should be maximized. This can be achieved by narrowing the band gap. The band gap engineering suggests a few methods for a decrease in the band gap energy, such as coupling of two or more semiconductors or doping with transition metals or non-metal. Moreover, the VBM (valence band maximum) and CBM (conduction band minimum) of the semiconductor need to be correlated with the redox potential of the catalysed reactions in order to make the reactions thermodynamically accessible upon photon absorption and guarantee the high efficiency of the treatment process. Tuning the band edge positions in the semiconductors can also be achieved by band gap engineering. For example, an increase in the energy of the VBM is possible by less electronegative anion substitutions if the VBM is dominated by O 2p states. Similarly, a decrease in the CBM energy can be reached by more electronegative transition metal cations substitutions if the CBM is dominated by empty metal d-states [222]. This requires the appropriate selection of the semiconductor modification in order to reach not only the change in the band edge position, but also the band gap narrowing.

Taking the fact that the semiconductor materials are applied as electrodes in the PEC treatment of wastewater into consideration, their active surface area should be high. It can be achieved by the application of nanostructured semiconductors in the form of nanotubes, nanowires, nanofibres, nanorods, and nanowalls. The nanostructured semiconductors can be easily obtained by electrochemical methods. The nanostructures are characterized not only by high surface area, but also by ability to minimize charge transfer recombination [84]. The surface area of the electrodes is connected with their catalytic activity, which should be improved in the case of semiconductors applied as photoelectrodes. This requires the lowering of the overpotential, which is related to the overall kinetic barrier to the photoelectrochemical reaction. The photoelectrode material should also be characterized by high conductivity. It also requires an appropriate modification of semiconductor materials, e.g., by dopants donating electron/hole carriers to the host materials without creating traps and with simultaneous reduction of activation barriers for carrier transfer [222]. When considering possible practical application of the PEC processes in wastewater treatment, the stability of semiconductor materials should also be taken into account. This parameter can seriously limit the practical application on a large scale. Although so many semiconductors were tested as photoelectrodes in the PEC treatment of various pollutants, only in a few cases, their stability was determined. Thus, accelerated stability tests seem to be necessary in the characterization of semiconductor materials. In this aspect, the substrates on which semiconductors are supported should also be properly selected and be characterized by high stability and conductivity. The preparation methods of photoelectrodes should be directed not only to their highest stability, activity, and conductivity, but also to the strong adherence of semiconductors to the conductive substrates.

The PEC processes of pollutants treatment with the application of semiconductor materials as photoelectrodes presented in this paper have some disadvantages. The long duration of treatment attracts attention in many cases. This results in a high energy consumption and high costs, making the PEC process questionable in practical use. Moreover, in many cases, the degradation efficiency of the PEC process was estimated as a decrease in pollutant concentration (sometimes only decolorization of a pollutant solution) without the determination of the final products, which can be toxic. The almost complete mineralisation of pollutant solutions was only achieved in few cases and usually required a significantly higher duration of the treatment process. Thus, a combination of the PEC process with other treatment methods, e.g., physicochemical or biological methods, is worth considering. This

should result in a reduction of operating costs as well as in shorter duration of the PEC process. In this case, the conversion of toxic and recalcitrant pollutants into biodegradable compounds that were achieved in the PEC process can be followed by the subsequent biological process.

Additionally, the chemical energy stored in industrial wastewater is often wasted. Thus, it is important to develop clean and efficient wastewater treatment methods for the simultaneous removal of pollutants and recovery of energy stored in the wastewater. A solution to this problem is an application of photoelectrochemical fuel cells with efficient semiconductor photoanodes and photocathodes. Furthermore, the pollutants that are present in the wastewater should be simultaneously degraded at the photoanode and photocathode. This process requires an application of appropriate semiconductor materials as photoelectrodes and optimization of the operational parameters. A combination of photoelectrocatalytic anode for the oxidation of organic pollutants and photoelectrocatalytic cathode for the reduction of inorganic pollutants should be developed and improved as an efficient and environmentally friendly approach to wastewater treatment.

In summary, the development of semiconductor materials that were applied as photoelectrodes in wastewater treatment should be directed to the utilization of sunlight irradiation and the increase in their photoelectrocatalytic activity in order to increase the rate of pollutants degradation and decrease the costs of the treatment. Moreover, the semiconductor photoanodes and photocathodes should facilitate simultaneous energy generation in order to make the treatment processes self-sufficient and enable their practical application.

Funding: This research received no external funding.

Conflicts of Interest: The author declares no conflict of interest.

References

1. Gude, V.G. Wastewater treatment of microbial fuel cells—An overview. *J. Clean. Prod.* **2016**, *24*, 2095–2111. [CrossRef]
2. Chonde, S.G. Microbial fuel cell: A new approach of wastewater treatment with power generation. *Int. J. Chem. Environ. Pharmaceut. Res.* **2014**, *5*, 8–12.
3. Chaturvedi, V.; Verma, P. Microbial fuel cell: A green approach for the utilization of waste for the generation of bioelectricity. *Bioresour. Bioprocess.* **2016**, *3*, 38. [CrossRef]
4. Araneda, I.; Tapia, N.F.; Allende, K.L.; Vargas, I.T. Constructed wetland-microbial fuel cells for sustainable greywater treatment. *Water* **2018**, *10*, 940. [CrossRef]
5. Tatinclaux, M.; Gregoire, K.; Leininger, A.; Biffinger, J.C.; Tender, L.; Ramirez, M.; Torrents, A.; Kjellerup, B.V. Electricity generation from wastewater using a floating air cathode microbial fuel cell. *Water Energy Nexus* **2018**, *1*, 97–103. [CrossRef]
6. Guadarrama-Perez, O.; Gutiererez-Macias, T.; Garcia-Sanchez, L.; Guadarrama-Perez, V.H.; Estrada-Arriaga, E.B. Recent advances in constructed wetland-microbial fuel cells for simultaneous bioelectricity production and wastewater treatment: A review. *Int. J. Energ. Res.* **2019**, *43*, 5106–5127. [CrossRef]
7. Antolini, E. Photoelectrocatalytic fuel cells and photoelectrode microbial fuel cells for wastewater treatment and power generation. *J. Environ. Chem. Eng.* **2019**, *7*, 103241. [CrossRef]
8. Wlodarczyk, P.P.; Wlodarczyk, B. Preparation and analysis of Ni-Co catalyst used for electricity production and COD reduction in microbial fuel cells. *Catalysts* **2019**, *9*, 1042. [CrossRef]
9. Osterloh, F.E.; Parkinson, B.A. Recent developments in solar water-splitting photocatalysis. *MRS Bull.* **2011**, *36*, 17–22. [CrossRef]
10. Habisreutinger, S.N.; Schmidt-Mende, L.; Stolarczyk, J.K. Photocatalytic reduction of CO_2 on TiO_2 and other semiconductors. *Angew. Chem. Int. Ed.* **2013**, *52*, 7372–7408. [CrossRef]
11. Li, J.; Wu, N. Semiconductor-based photocatalysts and photoelectrochemical cells for solar fuel generation: A review. *Catal. Sci. Technol.* **2015**, *5*, 1360–1384. [CrossRef]

12. Chen, X.; Chen, R.; Zhu, X.; Liao, Q.; Zhang, Y.; Ye, D.; Zhang, B.; Yu, Y.; Li, J. A solar responsive cubic nanosized CuS/Cu_2O/Cu photocathode with enhanced photoelectrochemical activity. *J. Catal.* **2019**, *372*, 182–192. [CrossRef]
13. Liang, H.; Jia, Z.; Zhang, H.; Wang, X.; Wang, J. Photocatalysis oxidation activity regulation of Ag/TiO_2 composites evaluated by the selective oxidation of Rhodamine B. *Appl. Surf. Sci.* **2017**, *422*, 1–10. [CrossRef]
14. Hu, Y.; Chen, W.; Fu, J.; Ba, M.; Sun, F.; Zhang, P.; Zou, J. Hydrothermal synthesis of $BiVO_4$/TiO_2 composites and their application for degradation of gaseous benzene under visible light irradiation. *Appl. Surf. Sci.* **2018**, *436*, 319–326. [CrossRef]
15. Di Paola, A.; Garcia-Lopez, E.; Marci, G.; Palmisano, L. A survey of photocatalytic materials for environmental remediation. *J. Hazard. Mater.* **2012**, *211*, 3–29. [CrossRef]
16. Brillas, E.; Martinez-Huitle, C.A. Decontamination of wastewaters containing synthetic organic dyes by electrochemical methods. An updated review. *Appl. Catal. B Environ.* **2015**, *166–167*, 603–643. [CrossRef]
17. Oturan, M.A.; Aaron, J.J. Advanced oxidation processes in water/wastewater treatment: Principles and applications. A review. *Crit. Rev. Environ. Sci. Technol.* **2014**, *44*, 2577–2641. [CrossRef]
18. Sires, I.; Brillas, E.; Oturan, M.A.; Rodrigo, M.A.; Panizza, M. Electrochemical advanced oxidation processes: Today and tomorrow. A review. *Environ. Sci. Pollut. Res.* **2014**, *21*, 8336–8367. [CrossRef]
19. Chaplin, B.P. Critical review of electrochemical advanced oxidation processes for water treatment applications. *Environ. Sci. Processes Impacts* **2014**, *16*, 1182–1203. [CrossRef]
20. Reyes-Gil, K.R.; Robinson, D.B. WO_3-enhanced TiO_2 Nanotube photoanodes for solar water splitting with simultaneous wastewater treatment. *Appl. Mater. Interfaces* **2013**, *5*, 12400–12410. [CrossRef]
21. Peleyeju, M.G.; Arotiba, O.A. Recent trends in visible-light photoelectrocatalytic systems for degradation of organic contaminants in water/wastewater. *Environ. Sci. Water Res. Technol.* **2018**, *4*, 1389–1411. [CrossRef]
22. Smith, Y.R.; Ray, R.S.; Carlson, K.; Sarma, B.; Misra, M. Self-ordered Titanium dioxide nanotube arrays: Anodic synthesis and their photo/electro-catalytic applications. *Materials* **2013**, *6*, 2892–2957. [CrossRef]
23. Liu, Y.; Gan, X.; Zhou, B.; Xiong, B.; Li, J.; Dong, C.; Bai, J.; Cai, W. Photoelectrocatalytic degradation of tetracycline by highly effective TiO_2 nanopore arrays electrode. *J. Hazard. Mater.* **2009**, *171*, 678–683. [CrossRef]
24. Kusmierek, E.; Chrzescijanska, E. Photoelectrochemical degradation of the reactive dye—Reactive Blue 81. *Pol. J. Chem.* **2009**, *83*, 1337–1351.
25. Rajeshwar, K. *Fundamentals of Semiconductor Electrochemistry and Photoelectrochemistry. Encyclopedia of Electrochemistry*; Viley-VCH Verlag: Hoboken, NJ, USA, 2007.
26. Yuan, R.; Ramjaun, S.N.; Wang, Z.; Liu, J. Photocatalytic degradation and chlorination of azo dye in saline wastewater: Kinetics and AOX formation. *Chem. Eng. J.* **2012**, *192*, 171–178. [CrossRef]
27. Tang, C.; Chen, V. The photocatalytic degradation of reactive black 5 using TiO_2/UV in an annular photoreactor. *Water Res.* **2004**, *38*, 2775–2781. [CrossRef]
28. Lopez-Grimau, V.; Gutierrez, M.C. Decolourisation of simulated reactive dyebath effluents by electrochemical oxidation assisted by UV light. *Chemosphere* **2006**, *62*, 106–112. [CrossRef]
29. Hepel, M.; Luo, J. Photoelectrochemical mineralization of textile diazo dye pollutants using nanocrystalline WO_3 electrodes. *Electrochim. Acta* **2001**, *47*, 729–740. [CrossRef]
30. Asahi, R.; Morikawa, T.; Irie, H.; Ohwaki, T. Nitrogen-doped titanium dioxide as visible-light-sensitive photocatalyst: Designs, developments, and prospects. *Chem. Rev.* **2014**, *114*, 9824–9852. [CrossRef]
31. Zhang, M.; Chen, C.; Ma, W.; Zhao, J. Visible-light-induced aerobic oxidation of alcohols in a coupled photocatalytic system of dye-sensitized TiO_2 and TEMPO. *Angew. Chem.* **2008**, *120*, 9876–9879. [CrossRef]
32. Casbeer, E.; Sharma, V.K.; Li, X.-Z. Synthesis and photocatalytic activity of ferrites under visible light: A review. *Sep. Purif. Technol.* **2012**, *87*, 1–14. [CrossRef]
33. Kanakaraju, D.; Glass, B.D.; Oelgemoller, M. Advanced oxidation process-mediated removal of pharmaceuticals from water: A review. *J. Environ. Manag.* **2018**, *219*, 189–207. [CrossRef]
34. Panizza, M.; Cerisola, G. Direct and mediated anodic oxidation of organic pollutants. *Chem. Rev.* **2009**, *109*, 6541–6569. [CrossRef]
35. Martinez-Huitle, C.A.; Ferro, S. Electrochemical oxidation of organic pollutants for the wastewater treatment: Direct and indirect processes. *Chem. Soc. Rev.* **2006**, *35*, 1324–1340. [CrossRef]
36. Janssen, L.J.J.; Koene, L. The role of electrochemistry and electrochemical technology in environmental protection. *Chem. Eng. J.* **2002**, *85*, 137–146. [CrossRef]

37. Ama, O.M.; Wilson, A.W.; Ray, S.S. Photoelectrochemical degradation of methylene blue dye under visible light irradiation using EG/Ag-ZrO_2 nanocomposite electrodes. *Int. J. Electrochem. Sci.* **2019**, *14*, 9982–10001.
38. Scott, K. *Electrochemical Processes for Clean Technology*; Royal Society of Chemistry, Thomas Graham House: Cambridge, UK, 1995.
39. Cavalcanti, E.B.; Garcia-Segura, S.; Centellas, F.; Brillas, E. Electrochemical incineration of omeprazole in neutral aqueous medium using a platinum or boron-doped diamond anode: Degradation kinetics and oxidation products. *Water Res.* **2013**, *47*, 1803–1815. [CrossRef]
40. Garcia-Segura, S.; Ocon, J.D.; Chong, M.N. Electrochemical oxidation remediation of real wastewater effluents—A review. *Process Saf. Environ. Prot.* **2018**, *113*, 48–67. [CrossRef]
41. Kapalka, A.; Foti, G.; Comninellis, C. The importance of electrode material in environmental electrochemistry. Formation and reactivity of free hydroxyl radicals on boron-doped diamond electrodes. *Electrochim. Acta.* **2009**, *54*, 2018–2023.
42. Tantis, I.; Antonopoulou, M.; Konstantinou, I.; Lianos, P. Coupling of electrochemical and photocatalytic technologies for accelerating degradation of organic pollutants. *J. Photochem. Photobiol. A* **2016**, *317*, 100–107. [CrossRef]
43. Su, Y.-F.; Wang, G.-B.; Kuo, D.T.F.; Chang, M.-L.; Shih, Y.-H. Photoelectrocatalytic degradation of antibiotic sulfamethoxazole using TiO_2/Ti photoanode. *Appl. Catal. B Environ.* **2016**, *186*, 184–192. [CrossRef]
44. Brillas, E.; Sires, I.; Cabot, P.L. Use of both anode and cathode reactions in wastewater treatment. Chapter 19. In *Electrochemistry for the Environment*; Comninellis, C., Chen, G., Eds.; Springer: Berlin/Heidelberg, Germany, 2010; pp. 515–551.
45. Panizza, M.; Cerisola, G. Application of diamond electrodes to electrochemical processes. *Electrochim. Acta* **2005**, *51*, 191–199. [CrossRef]
46. Valatka, E.; Kulesius, Z. TiO_2-mediated photoelectrochemical decoloration of methylene blue in the presence of peroxodisulfate. *J. Appl. Electrochem.* **2007**, *37*, 415–420. [CrossRef]
47. Avetta, P.; Pensato, A.; Minella, M.; Malandrino, M.; Maurino, V.; Minero, C.; Hanna, K.; Vione, D. Activation of persulfate by irradiated magnetite: Implications for the degradation of phenol under heterogeneous photo-Fenton-like conditions. *Environ. Sci. Technol.* **2015**, *49*, 1043–1050. [CrossRef] [PubMed]
48. Capodaglio, A.G. Contaminants of emerging concern removal by high-energy oxidation-reduction processes: State of the art. *Appl. Sci.* **2019**, *9*, 4562. [CrossRef]
49. Armstrong, D.A.; Huie, R.E.; Lymar, S.; Koppenol, W.H.; Merenyi, G.; Neta, P.; Stanbury, D.M.; Steenken, S.; Wardman, P. Standard electrode potentials involving radicals in aqueous solution: Inorganic radicals. *BioInorg. React. Mech.* **2013**, *9*, 59–61. [CrossRef]
50. Meng, X.; Zhang, Z.; Li, X. Synergetic photoelectrocatalytic reactors for environmental remediation: A review. *J. Photochem. Photobiol. C* **2015**, *24*, 83–101. [CrossRef]
51. Bessegato, G.G.; Guaraldo, T.T.; de Brito, J.F.; Brugnera, M.F.; Zanoni, M.V.B. Achievements and trends in photoelectrocatalysis: From environmental to energy applications. *Electrocatalysis* **2015**, *6*, 415–441. [CrossRef]
52. Ren, K.; Gan, Y.X. Advances in photoelectrochemical fuel cell research. Chapter 1. In *Small-Scale Energy Harvesting*; Lallart, M., Ed.; IntechOpen: London, UK, 2012; pp. 3–26.
53. Zarei, E.; Ojani, R. Fundamentals and some applications of photoelectrocatalysis and effective factors on its efficiency: A review. *J. Solid State Electrochem.* **2017**, *21*, 305–336. [CrossRef]
54. Dahrir, R.; Drogui, P.; Robert, D. Photoelectrocatalytic technologies for environmental applications. *J. Photochem. Photobiol. A* **2012**, *238*, 41–52. [CrossRef]
55. Wang, N.; Li, X.; Wang, Y.; Quan, X.; Chen, G. Evaluation of bias potential enhanced photocatalytic degradation of 4-chlorophenol with TiO_2 nanotube fabricated by anodic oxidation method. *Chem. Eng. J.* **2009**, *146*, 30–35. [CrossRef]
56. Quan, X.; Ruan, X.; Zhao, H.; Chen, S.; Zhao, Y. Photoelectrocatalytic degradation of pentachlorophenol in aqueous solution using a TiO_2 nanotube film electrode. *Environ. Pollut.* **2007**, *147*, 409–414. [CrossRef]
57. Zanoni, M.V.B.; Sene, J.J.; Anderson, M.A. Photoelectrocatalytic degradation of Remazol Brilliant Orange 3R on titanium dioxide thin-film electrodes. *J. Photochem. Photobiol. A* **2003**, *157*, 55–63. [CrossRef]
58. Candal, R.J.; Zeltner, W.A.; Anderson, M.A. Effects of pH and applied potential on photocurrent and oxidation rate of saline solutions of formic acid in a photoelectrocatalytic reactor. *Environ. Sci. Technol.* **2000**, *34*, 3443–3451. [CrossRef]

59. Zhou, X.; Zheng, Y.; Zhou, J.; Zhou, S. Degradation kinetics of photoelectrocatalysis on landfill leachate using codoped TiO_2/Ti photoelectrodes. *J. Nanomater.* **2015**, *2015*, 810579. [CrossRef]
60. Konstantinou, I.K.; Albanis, T.A. TiO_2-assisted photocatalytic degradation of azo dyes in aqueous solution: Kinetic and mechanistic investigations. A review. *Appl. Catal. B Environ.* **2004**, *49*, 1–14. [CrossRef]
61. Chen, H.; Li, J.; Chen, Q.; Li, D.; Zhou, B. Photoelectrocatalytic performance of benzoic acid on TiO_2 nanotube array electrodes. *Int. J. Photoenergy* **2013**, *2013*, 567426. [CrossRef]
62. Wang, W.-Y.; Yang, M.-L.; Ku, Y. Photoelectrocatalytic decomposition of dye in aqueous solution using Nafion as an electrolyte. *Chem. Eng. J.* **2010**, *165*, 273–280. [CrossRef]
63. Zhang, Y.; Xiong, X.; Han, Y.; Zhang, X.; Shen, F.; Deng, S.; Xiao, H.; Yang, X.; Yang, G.; Peng, H. Photoelectrocatalytic degradation of recalcitrant organic pollutants using TiO_2 film electrodes: An overview. *Chemosphere* **2012**, *88*, 145–154. [CrossRef]
64. Yang, L.; Liu, Z. Study on light intensity in the process of photocatalytic degradation of indoor gaseous formaldehyde for saving energy. *Energy Convers. Manag.* **2007**, *48*, 882–889. [CrossRef]
65. Amama, P.B.; Itoh, K.; Murabayashi, M. Gas-phase photocatalytic degradation of trichloroethylene on pretreated TiO_2. *Appl. Catal. B Environ.* **2002**, *37*, 321–330. [CrossRef]
66. Pareek, V.; Chong, S.; Tade, M.; Adesina, A.A. Light intensity distribution in heterogeneous photocatalytic reactors. *Asia-Pac. J. Chem. Eng.* **2008**, *3*, 171–201. [CrossRef]
67. Mahmoodi, N.M.; Arami, M. Degradation and toxicity reduction of textile wastewater using immobilized titania nanophotocatalysis. *J. Photochem. Photobiol. B* **2009**, *94*, 20–24. [CrossRef]
68. Hu, C.; Yu, J.C.; Hao, Z.; Wong, P.K. Photocatalytic degradation of triazine-containing azo dyes in aqueous TiO_2 suspensions. *Appl. Catal. B Environ.* **2003**, *42*, 47–55. [CrossRef]
69. Wang, K.-S.; Chen, H.-Y.; Huang, L.-C.; Su, Y.-C.; Chang, S.-H. Degradation of Reactive Black 5 using combined electrochemical degradation-solar-light/immobilized TiO_2 film process and toxicity evaluation. *Chemosphere* **2008**, *72*, 299–305. [CrossRef]
70. Gao, B.; Yap, P.S.; Lim, T.M.; Lim, T.-T. Adsorption-photocatalytic degradation of Acid Red 88 by supported TiO_2: Effect of activated carbon support and aqueous anions. *Chem. Eng. J.* **2011**, *171*, 1098–1107. [CrossRef]
71. Mahmoodi, N.M.; Arami, M.; Limaee, N.Y. Photocatalytic degradation of triazinic ring-containing azo dye (Reactive Red 198) by using immobilized TiO_2 photoreactor: Bench scale study. *J. Hazard. Mater.* **2006**, *B133*, 113–118. [CrossRef]
72. Nadarajan, R.; Bakar, W.A.W.A.; Ali, R.; Ismail, R. Photocatalytic degradation of 1,2-dichlorobenzene using immobilized TiO_2/SnO_2/WO_3 photocatalyst under visible light: Application of response surface methodology. *Arab. J. Chem.* **2018**, *11*, 34–47. [CrossRef]
73. Zhang, L.; Ran, J.; Qiao, S.-Z.; Jaroniec, M. Characterization of semiconductor photocatalysts. *Chem. Soc. Rev.* **2019**, *48*, 5184–5206. [CrossRef]
74. Esquivel, K.; Arriaga, L.G.; Rodriguez, F.J.; Martinez, L.; Godinez, L.A. Development of a TiO_2 modified optical fiber electrode and its incorporation into a photoelectrochemical reactor for wastewater treatment. *Water Res.* **2009**, *43*, 3593–3603. [CrossRef]
75. Sun, R.; Zhang, Z.; Li, Z.; Jing, L. Review on photogenerated hole modulation strategies in photoelectrocatalysis for solar fuel production. *ChemCatChem* **2019**, *11*, 5875–5884. [CrossRef]
76. Georgieva, J.; Valova, E.; Armyanov, S.; Philippidis, N.; Poulios, I.; Sotiropoulos, S. Bi-component semiconductor oxide photoanodes for the photoelectrocatalytic oxidation of organic solutes and vapours: A short review with emphasis to TiO_2-WO_3 photoanodes. *J. Hazard. Mater.* **2012**, *211-212*, 30–46. [CrossRef]
77. Egerton, T.A. Does photoelectrocatalysis by TiO_2 work? *J. Chem. Technol. Biotechnol.* **2011**, *86*, 1024–1031. [CrossRef]
78. Deng, Y.; Zhao, R. Advanced oxidation processes (AOPs) in wastewater treatment. *Curr. Pollut. Rep.* **2015**, *1*, 167–176. [CrossRef]
79. Tabai, A.; Bechiri, O.; Abbessi, M. Degradation of organic dye using a new homogeneous Fenton-like system based on hydrogen peroxide and a recyclable Dawson-type heteropolyanion. *Int. J. Ind. Chem.* **2017**, *8*, 83–89. [CrossRef]
80. Eren, Z. Degradation of an azo dye with homogeneous and heterogeneous catalysts by sonophotolysis. *Clean Soil Air Water* **2012**, *40*, 1284–1289. [CrossRef]

81. Ama, O.M.; Mabuba, N.; Arotiba, O.A. Synthesis, characterization and application of exfoliated graphite/zirconium nanocomposite electrode for the photoelectrochemical degradation of organic dye in water. *Electrocatalysis* **2015**, *6*, 390–397. [CrossRef]
82. Paramasivam, I.; Jha, H.; Liu, N.; Schmuki, P. A review of photocatalysis using self-organized TiO_2 nanotubes and other ordered oxide nanostructures. *Small* **2012**, *8*, 3073–3103. [CrossRef]
83. Kunst, M.; Goubard, F.; Colbeau-Justin, C.; Wunsch, F. Electronic transport in semiconductor nanoparticles for photocatalytic and photovoltaic applications. *Mater. Sci. Eng. C* **2008**, *27*, 1061–1064. [CrossRef]
84. Bessegato, G.G.; Guaraldo, T.T.; Zanoni, M.V.B. Enhancement of photoelectrocatalysis efficiency by using nanostructure electrodes. Chapter 10. In *Modern Electrochemical Methods in Nano, Surface and Corrosion Science*; Aliokhazraei, M., Ed.; IntechOpen: London, UK, 2014; pp. 271–319.
85. Peter, L.M. Photoelectrochemistry from basic principles to photocatalysis. Chapter 1. In *Photocatalysis: Fundamentals and Perspectives*; Schneider, J., Bahnemann, D., Ye, J., Puma, G.L., Dionysiou, D.D., Eds.; Royal Society of Chemistry: London, UK, 2016; pp. 3–28.
86. Bredas, J.-C. Mind the gap! *Mater. Horiz.* **2014**, *1*, 17–19. [CrossRef]
87. Le Bahers, T.; Takanbe, K. Combined theoretical and experimental characterizations of semiconductors for photoelectrocatalytic applications. *J. Photochem. Photobiol. C* **2019**, *40*, 212–233. [CrossRef]
88. Guijarro, N.; Prevot, M.S.; Sivula, K. Surface modification of semiconductor photoelectrodes. *Phys. Chem. Chem. Phys.* **2015**, *17*, 15655–15674. [CrossRef]
89. Brugnera, M.F.; de Araujo Souza, B.C.; Zanoni, M.V.B. Advanced oxidation processes applied to actinobacterium disinfection. Chapter 15. In *Antibacteria—Basics and Biotechnological Applications*; Dhanasekaran, D., Ed.; IntechOpen: London, UK, 2016; pp. 353–376.
90. Lee, M.-H.; Chang, K.-H.; Lin, H.-C. Effective density-of-states distribution of polycrystalline silicon thin-film transistors under hot-carrier degradation. *J. Appl. Phys.* **2007**, *102*, 0540508. [CrossRef]
91. Garcia-Esparza, A.T.; Takanabe, K. A simplified theoretical guideline for overall water splitting using photocatalyst particles. *J. Mater. Chem. A* **2016**, *4*, 2894–2908. [CrossRef]
92. Fernandez-Domene, R.M.; Rosello-Marquez, G.; Sanchez-Tovae, R.; Lucas-Granados, B. Photoelectrochemical removal of chlorfenvinphos by using WO_3 nanorods: Influence of annealing temperature and operation pH. *Sep. Purif. Technol.* **2019**, *212*, 458–464. [CrossRef]
93. Lei, Y.; Huo, J. Enhanced visible-light photoelectrocatalytic activity of nano-TiO_2/polyimide/Ni foam photoanode. *Res. Chem. Intermed.* **2018**, *44*, 6401–6418. [CrossRef]
94. Shen, Q.; Chen, Z.; Huang, X.; Liu, M.; Zhao, G. High-yield and selective photoelectrocatalytic reduction of CO_2 to formate by metallic copper decorated Co_3O_4 nanotube arrays. *Environ. Sci. Technol.* **2015**, *49*, 5828–5835. [CrossRef]
95. Paschoal, F.M.; Nunez, L.; de Vasconcelos Lanza, M.R.; Zanoni, M.V.B. Nitrate removal on a Cu/Cu_2O photocathode under UV irradiation and bias potential. *J. Adv. Oxid. Technol.* **2013**, *16*, 63–70. [CrossRef]
96. Rather, R.A.; Lo, I.M.C. Photoelectrochemical sewage treatment by a multifunctional g-C_3N_4/Ag/AgCl/$BiVO_4$ photoanode for the simultaneous degradation of emerging pollutants and hydrogen production, and the disinfection of *E. coli*. *Water Res.* **2020**, *168*, 115166. [CrossRef]
97. Rahmawati, F.; Kusumaningsih, T.; Hastuti, A. Photo- and electro-catalysis for solar disinfection of *Escherichia coli*-contaminated water using Ag-TiO_2/graphite. *Toxicol. Environ. Chem.* **2011**, *93*, 1602–1612. [CrossRef]
98. Brugnera, M.F.; Miyata, M.; Zocolo, G.J.; Leite, C.Q.F.; Zanoni, M.V.B. A photoelectrocatalytic process that disinfects water contaminated with *Mycobacterium kansasii* and *Mycobacterium avium*. *Water Res.* **2013**, *47*, 6596–6605. [CrossRef]
99. Wang, D.; Li, Y.; Puma, G.L.; Lianos, P.; Wang, C.; Wang, P. Photoelectrochemical cell for simultaneous electricity generation and heavy metals recovery from wastewater. *J. Hazard. Mater.* **2017**, *323*, 681–689. [CrossRef]
100. Mao, R.; Di, S.; Wang, Y.; Zhao, X. Photoelectrocatalytic degradation of Ag-cyanide complexes and synchronous recovery of metallic Ag driven by TiO_2 nanorods array photoanode combined with titanium cathode. *Chemosphere* **2020**, *242*, 125156. [CrossRef]
101. Hidalgo, K.T.S.; Ortiz-Quiles, E.O.; Betancourt, L.E.; Larios, E.; Jose-Yacaman, M.; Cabrera, C.R. Photoelectrochemical solar cells prepared from nanoscale zerovalent iron used for aqueous Cd^{2+} removal. *ACS Sustain. Chem. Eng.* **2016**, *4*, 738–745. [CrossRef]

102. Wang, Q.; Shi, X.; Liu, E.; Xu, J.; Crittenden, J.C.; Zhang, Y.; Cong, Y. Preparation and photoelectrochemical performance of visible-light active AgI/TiO_2-NTs composite with rich β-AgI. *Ind. Chem. Eng. Res.* **2016**, *55*, 4897–4904. [CrossRef]
103. Koo, M.K.; Cho, K.; Yoon, J.; Choi, W. Photoelectrochemical degradation of organic compounds coupled with molecular hydrogen generation using electrochromic TiO_2 nanotube arrays. *Environ. Sci. Technol.* **2017**, *51*, 6590–6598. [CrossRef]
104. Demir, M.E.; Chehade, G.; Dincer, I.; Yuzer, B.; Selcuk, H. Synergistic effects of advanced reactions in a combination of TiO_2 photocatalysis for hydrogen production and wastewater treatment applications. *Int. J. Hydrog. Energy* **2019**, *44*, 23856–23867. [CrossRef]
105. Han, H.-X.; Shi, C.; Yuan, L.; Sheng, G.-P. Enhancement of methyl orange degradation and power generation in a photoelectrocatalytic microbial fuel cell. *Appl. Energy* **2017**, *204*, 382–389. [CrossRef]
106. Shan, A.Y.; Ghazi, T.I.M.; Rashid, S.A. Immobilisation of titanium dioxide onto supporting materials in heterogeneous photocatalysis: A review. *Appl. Catal. A Gen.* **2010**, *389*, 1–8. [CrossRef]
107. Zhang, H.; Chen, G.; Bahnemann, D.W. Environmental photo(electro)catalysis: Fundamentals. Chapter 16. In *Electrochemistry for the Environment*; Comninellis, C., Chen, G., Eds.; Springer: Berlin/Heidelberg, Germany, 2010; pp. 371–442.
108. Zhang, M.; Chen, T.; Wang, Y. Insights into TiO_2 polymorphs: Highly selective synthesis, phase transition, and their polymorph-dependent properties. *RSC Adv.* **2017**, *7*, 52755–52761. [CrossRef]
109. Hanaor, D.A.H.; Sorrell, C.C. Review of the anatase to rutile phase transformation. *J. Mater. Sci.* **2011**, *46*, 855–874. [CrossRef]
110. Andronic, L.; Duta, A. TiO_2 thin films for dyes photodegradation. *Thin Solid Films* **2007**, *515*, 6294–6297. [CrossRef]
111. Du, Y.; Feng, Y.; Qu, Y.; Liu, J.; Ren, N.; Liu, H. Electricity generation and pollutant degradation using a novel bicathode coupled photoelectrochemical cell. *Environ. Sci. Technol.* **2014**, *48*, 7634–7641. [CrossRef]
112. Zhang, A.; Zhou, M.; Liu, L.; Jiao, Y.; Zhou, Q. A novel photoelectrocatalytic system for organic contaminant degradation on a TiO_2 nanotube (TNT)/Ti electrode. *Electrochim. Acta* **2010**, *55*, 5091–5099. [CrossRef]
113. Liu, Y.; Li, J.; Zhou, B.; Bai, J.; Zheng, Q.; Zhang, J.; Cai, W. Comparison of photoelectrochemical properties of TiO_2-nanotube-array photoanode prepared by anodization of different electrolyte. *Environ. Chem. Lett.* **2009**, *7*, 363–368. [CrossRef]
114. Xie, Y.B.; Li, X.Z. Interactive oxidation of photoelectrocatalysis and electro-Fenton for azo-dye degradation using TiO_2-Ti mesh and reticulated vitreous carbon electrodes. *Mater. Chem. Phys.* **2006**, *95*, 39–50. [CrossRef]
115. Liu, C.-F.; Huang, C.P.; Hu, C.-C.; Juang, Y.; Huang, C. Photoelectrochemical degradation of dye wastewater on TiO_2-coated titanium electrode prepared by electrophoretic deposition. *Sep. Purif. Technol.* **2016**, *165*, 145–153. [CrossRef]
116. Lin, W.-C.; Chen, C.-H.; Tang, H.-Y.; Hsiao, Y.-C.; Pan, J.R.; Hu, C.-C.; Huang, C. Electrochemical photocatalytic degradation of dye solution with a TiO_2-coated stainless steel electrode prepared by electrophoretic deposition. *Appl. Catal. B Environ.* **2013**, *140–141*, 32–41. [CrossRef]
117. Juang, y.; Liu, Y.; Nurhayati, E.; Thuy, N.T.; Huang, C.; Hu, C.-C. Anodic fabrication of advanced titania nanotubes photocatalysts for photoelectrocatalysis decolorization of Orange G dye. *Chemosphere* **2016**, *144*, 2462–2468. [CrossRef]
118. Ama, O.M.; Arotiba, O.A. Exfoliated graphite/titanium dioxide for enhanced photoelectrochemical degradation of methylene blue dye under simulated visible light irradiation. *J. Electroanal. Chem.* **2017**, *803*, 157–164. [CrossRef]
119. Garcia-Segura, S.; Dosta, S.; Guilemany, J.M.; Brillas, E. Solar photoelectrocatalytic degradation of Acid Orange 7 azo dye using a highly stable TiO_2 photoanode synthesized by atmospheric plasma spray. *Appl. Catal. B Environ.* **2013**, *132–133*, 142–150. [CrossRef]
120. Isaev, A.B.; Aliev, Z.M.; Adamadzieva, N.A. Photoelectrochemical oxidation of C.I. Direct Black 22 azo dye under elevated oxygen pressure. *Russ. J. Appl. Chem.* **2012**, *85*, 765–769. [CrossRef]
121. Franz, S.; Perego, D.; Marchese, O.; Bestetti, M. Photoelectrochemical advanced oxidation processes of nanostructured TiO_2 catalysts: Decolorization of a textile azo-dye. *J. Water Chem. Technol.* **2015**, *37*, 108–115. [CrossRef]
122. Tan, B.; Zhang, Y.; Long, M. Large-scale preparation of nanoporous TiO_2 film on titanium substrate with improved photoelectrochemical performance. *Nanoscale Res. Lett.* **2014**, *9*, 190. [CrossRef] [PubMed]

123. Villota-Zuleta, J.A.; Rodriguez-Acosta, J.W.; Castilla-Acevedo, S.F.; Marriaga-Cabrales, N.; Machuca-Martinez, F. Experimental data on the photoelectrochemical oxidation of phenol: Analysis of pH, potential and initial concentration. *Data in Brief* **2019**, *24*, 103949. [CrossRef]
124. Bennani, Y.; Appel, P.; Rietveld, L.C. Optimisation of parameters in a solar light induced photoelectrocatalytic process with a TiO_2 composite electrode prepared by paint thermal decomposition. *J. Photochem. Photobiol. A* **2015**, *305*, 83–92. [CrossRef]
125. Li, X.Z.; Liu, H.S. Development of an E-H_2O_2/TiO_2 photoelectrocatalytic oxidation system for water and wastewater treatment. *Environ. Sci. Technol.* **2005**, *39*, 4614–4620. [CrossRef]
126. Liu, Z.; Zhang, X.; Nishimoto, S.; Jin, M.; Tryk, D.A.; Murakami, T.; Fujishima, A. Highly ordered TiO_2 nanotube arrays with controllable length for photoelectrocatalytic degradation of phenol. *J. Phys. Chem. C* **2008**, *112*, 253–259. [CrossRef]
127. Tian, M.; Wu, G.; Adams, B.; Wen, J.; Chen, A. Kinetics of photoelectrocatalytic degradation on nitrophenols on nanostructured TiO_2 electrodes. *J. Phys. Chem. C* **2008**, *112*, 825–831. [CrossRef]
128. Enright, P.; Betts, A.; Cassidy, J. A practical photoelectrochemical cell using non precious metal electrodes. *J. Appl. Electrochem.* **2011**, *41*, 345–353. [CrossRef]
129. Daskalaki, V.; Fulgione, I.; Frontistis, Z.; Rizzo, L.; Mantzavinos, D. Solar light-induced photoelectrocatalytic degradation of bisphenol-A on TiO_2/ITO film anode and BDD cathode. *Catal. Today* **2013**, *209*, 74–78. [CrossRef]
130. Montenegro-Ayo, R.; Morales-Gomero, J.C.; Alarcon, H.; Cotillas, S.; Westerhoff, P.; Garcia-Segura, S. Scaling up photoelectrocatalytic reactors: A TiO_2 nanotube-coated disc compound reactor effectively degrades acetaminophen. *Water* **2019**, *11*, 2522. [CrossRef]
131. Peleyeju, M.G.; Umukoro, E.H.; Tshwenya, L.; Moutloali, R.; Babalola, J.O.; Arotiba, O.A. Photoelectrocatalytic water treatment systems: Degradation, kinetics and intermediate products studies of sulfamethoxazole on a TiO_2-exfoliated graphite electrode. *RSC Adv.* **2017**, *7*, 40571–40580. [CrossRef]
132. Komtchou, S.; Dirany, A.; Drogui, P.; Delegan, N.; El Khakani, M.A.; Robert, D.; Lafrance, P. Degradation of atrazine in aqueous solution with electrophotocatalytic process using TiO_{2-x} photoanode. *Chemosphere* **2016**, *157*, 79–88. [CrossRef] [PubMed]
133. Wang, Z.; Yang, C.; Lin, T.; Yin, H.; Chen, P.; Wan, D.; Xu, F.; Huang, F.; Lin, J.; Xie, X.; et al. Visible light photocatalytic, solar thermal and photoelectrochemical properties of aluminium-reduced black titania. *Energy Environ. Sci.* **2013**, *6*, 3007–3014. [CrossRef]
134. Bai, J.; Liu, Y.; Li, J.; Zhou, B.; Zheng, Q.; Cai, W. A novel thin layer photoelectrocatalytic (PEC) reactor with double-faced titania nanotube arrays electrode for effective degradation of tetracycline. *Appl. Catal. B Environ.* **2010**, *98*, 154–160. [CrossRef]
135. Daghrir, R.; Drogui, P.; El Khakani, M.A. Photoelectrocatalytic oxidation of chlortetracycline using Ti/TiO_2 photo-anode with simultaneous H_2O_2 production. *Electrochim. Acta* **2013**, *87*, 18–31. [CrossRef]
136. Daghrir, R.; Drogui, P.; Dimboukou-Mpira, A.; El Khakani, M.A. Photoelectrocatalytic degradation of carbamazepine using Ti/TiO_2 nanostructured electrodes deposited by means of a pulsed laser deposition process. *Chemosphere* **2013**, *93*, 2756–2766. [CrossRef]
137. Paschoal, F.M.M.; Anderson, M.A.; Zanoni, M.V.B. Photoelectrocatalytic oxidation of anionic surfactant used in leather industry on nanoporous Ti/TiO_2 electrodes. *J Braz. Chem. Soc.* **2008**, *19*, 803–810. [CrossRef]
138. Wang, Q.; Shang, J.; Zhu, T.; Zhao, F. Efficient photoelectrocatalytic reduction of Cr(VI) using TiO_2 nanotube arrays as the photoanode and a large-area titanium mesh as the photocathode. *J. Mol. Catal. A Chem.* **2011**, *335*, 242–247. [CrossRef]
139. He, H.; Zong, M.; Dong, F.; Yang, P.; Ke, G.; Liu, M.; Nie, X.; Ren, W.; Bian, L. Simultaneous removal and recovery of uranium from aqueous solution using TiO_2 photoelectrochemical reduction method. *J. Radioanal. Nucl. Chem.* **2017**, *313*, 59–67. [CrossRef]
140. Fang, T.; Liao, L.; Xu, X.; Peng, J.; Jing, Y. Removal of COD and color in real pharmaceutical wastewater by photoelectrocatalytic oxidation method. *Environ. Technol.* **2013**, *34*, 779–786. [CrossRef]
141. Li, K.; Zhang, H.; Ma, Y.; Sun, T.; Jia, J. Nanostructured polypyrrole cathode based dual rotating disk photo fuel cell for textile wastewater purification and electricity generation. *Electrochim. Acta* **2019**, *303*, 329–340. [CrossRef]
142. Babu, B.R.; Parande, A.K.; Raghu, S.; Kumar, T.P. Cotton textile processing: Waste generation and effluent treatment. *J. Cotton Sci.* **2007**, *11*, 141–153.

143. Asmussen, R.M.; Tian, M.; Chen, A. A new approach to wastewater remediation based on bifunctional electrodes. *Environ. Sci. Technol.* **2009**, *43*, 5100–5105. [CrossRef]
144. Bolton, J.R.; Bircher, K.G.; Tumas, W.; Tolman, A.A. Figures-of-merit for the technical development and application of advanced oxidation technologies for both electric- and solar-driven systems. *Pure Appl. Chem.* **2001**, *73*, 627–637. [CrossRef]
145. Zhang, H.; Chen, G.; Bahnemann, D.W. Photoelectrocatalytic materials for environmental applications. *J. Mater. Chem.* **2009**, *19*, 5089–5121. [CrossRef]
146. Yazyev, O.V.; Kis, A. MoS_2 and semiconductors in the flatland. *Mater. Today* **2015**, *18*, 20–30. [CrossRef]
147. Bandaru, S.; Saranaya, G.; English, N.J.; Yam, C.; Chen, M. Tweaking the electronic and optical properties of α-MoO_3 by sulphur and selenium doping—A density functional theory study. *Sci. Rep.* **2018**, *8*, 10144. [CrossRef]
148. Inzani, K.; Nematollahi, M.; Vullum-Bruer, F.; Grande, T.; Reenaas, T.W.; Selbach, S.M. Electronic properties of reduced molybdenum oxides. *Phys. Chem. Chem. Phys.* **2017**, *19*, 9232–9245. [CrossRef]
149. Sinhamahapatra, A.; Jeon, J.-P.; Kang, J.; Han, B.; Yu, J.-S. Oxygen-deficient zirconia (ZrO_{2-x}): A new material for solar light absorption. *Sci. Rep.* **2016**, *6*, 27218. [CrossRef]
150. Walsh, A.; Yan, Y.; Huda, M.N.; Al-Jassim, M.M.; Wei, S.-H. Band edge electronic structure of $BiVO_4$: Elucidating the role of the Bi s and V d orbitals. *Chem. Mater.* **2009**, *21*, 547–551. [CrossRef]
151. Cao, J.; Zhou, C.; Lin, H.; Xu, B.; Chen, S. Surface modification of *m*-$BiVO_4$ with wide band-gap semiconductor BiOCl to largely improve the visible light induced photocatalytic activity. *Appl. Surf. Sci.* **2013**, *284*, 263–269. [CrossRef]
152. He, Q.; Ni, Y.; Ye, S. Heterostructured Bi_2O_3/Bi_2MoO_6 nanocomposites: Simple construction and enhanced visible-light photocatalytic performance. *RSC Adv.* **2017**, *7*, 27089–27099. [CrossRef]
153. Alfaifi, B.Y.; Tahir, A.A.; Wijayantha, K.G.U. Fabrication of Bi_2WO_6 photoelectrodes with enhanced photoelectrochemical and photocatalytic performance. *Sol. Energy Mater. Sol. Cells* **2019**, *195*, 134–141. [CrossRef]
154. Mishra, M.; Chun, D.-M. α-Fe_2O_3 as a photocatalytic material: A review. *Appl. Catal. A Gen.* **2015**, *498*, 126–141. [CrossRef]
155. Zhang, M.; Pu, W.; Pan, S.; Okoth, O.K.; Yang, C.; Zhang, J. Photoelectrocatalytic activity of liquid phase deposited α-Fe_2O_3 films under visible light illumination. *J. Alloys Compd.* **2015**, *648*, 719–725. [CrossRef]
156. Toma, F.M.; Cooper, J.K.; Kunzelmann, V.; McDowell, M.T.; Yu, J.; Larson, D.M.; Borys, N.J.; Abelyan, C.; Beeman, J.W.; Yu, K.M.; et al. Mechanistic insights into chemical and photochemical transformations of bismuth vanadate photoanodes. *Nat. Commun.* **2016**, *7*, 12012. [CrossRef]
157. Wang, K.; He, H.; Li, D.; Li, Y.; Li, J.; Li, W. Photoelectrochemical reduction of Cr (VI) on plate-like WO_3/$BiVO_4$ composite electrodes under visible-light irradiation: Characteristics and kinetic study. *J. Photochem. Photobiol. A* **2018**, *367*, 438–445. [CrossRef]
158. Luo, J.-Y.; Chen, L.-L.; Liang, X.-H.; Zhao, Q.-W.; Li, H. Anodic deposition-assisted photoelectrocatalytic degradation of bisphenol A at a cadmium sulphide modified electrode based on visible light-driven fuel cells. *Electrochim. Acta* **2015**, *186*, 420–426. [CrossRef]
159. Kim, G.; Igunnu, E.T.; Chen, G.Z. A sunlight assisted dual purpose photoelectrochemical cell for low voltage removal of heavy metals and organic pollutants in wastewater. *Chem. Eng. J.* **2014**, *244*, 411–421. [CrossRef]
160. Umukoro, E.H.; Peleyeju, M.G.; Ngila, J.C.; Arotiba, O.A. Towards wastewater treatment: Photo-assisted electrochemical degradation of 2-nitrophenol and orange II dye at a tungsten trioxide-exfoliated graphite composite electrode. *Chem. Eng. J.* **2017**, *317*, 290–301. [CrossRef]
161. Shen, Z.; Li, J.; Zhang, Y.; Bai, J.; Tan, X.; Li, X.; Qiao, L.; Xu, Q.; Zhou, B. Highly efficient total nitrogen and simultaneous total organic carbon removal for urine based on the photoelectrochemical cycle reaction of chlorine and hydroxyl radicals. *Electrochim. Acta* **2019**, *297*, 1–9. [CrossRef]
162. Chen, Q.; Li, J.; Li, X.; Huang, K.; Zhou, B.; Cai, W.; Shangguan, W. Visible-light responsive photocatalytic fuell cell based on WO_3/W photoanode and Cu_2O/Cu photocathode for simultaneous wastewater treatment and electricity generation. *Environ. Sci. Technol.* **2012**, *46*, 11451–11458. [CrossRef] [PubMed]
163. Zheng, Q.; Lee, C. Visible light photoelectrocatalytic degradation of methyl orange using anodized nanoporous WO_3. *Electrochim. Acta* **2014**, *115*, 140–145. [CrossRef]

164. Fernandez-Domene, R.M.; Sanchez-Tovar, R.; Lucas-Granados, B.; Munoz-Portero, M.J. Elimination of pesticide atrazine by photoelectrocatalysis using a photoanode based on WO_3 nanosheets. *Chem. Eng. J.* **2018**, *350*, 1114–1124. [CrossRef]
165. Wang, T.; Lin, c.-A.; Xu, S.; Wang, C.-F.; Chen, C.-W.; Dong, C.-D. Toward concurrent organics removal and potential hydrogen production in wastewater treatment: Photoelectrochemical decolorization of methylene blue over hematite electrode in the presence of Mn(I). *Appl. Catal. B Environ.* **2019**, *244*, 140–149. [CrossRef]
166. Fan, X.; Zhou, Y.; Zhang, G.; Liu, T.; Dong, W. In situ photoelectrochemical activation of sulphite by MoS_2 photoanode for enhanced removal of ammonium nitrogen from wastewater. *Appl. Catal. B Environ.* **2019**, *244*, 396–406. [CrossRef]
167. Sapkal, R.T.; Shinde, S.S.; Mahadik, M.A.; Mohite, V.S.; Waghmode, T.R.; Govindwar, S.P.; Rajpure, K.Y.; Bhosale, C.H. Photoelectrocatalytic decolorization and degradation of textile effluent using ZnO thin films. *J. Photochem. Photobiol. B* **2012**, *114*, 102–107. [CrossRef]
168. Ntsedwana, B.; Sampath, S.; Mamba, B.B.; Oluwafemi, O.S.; Arotiba, O.A. Photoelectrochemical degradation of eosin yellowish dye on exfoliated graphite-ZnO nanocomposite electrode. *J. Mater. Sci. Mater. Electron.* **2016**, *27*, 592–598. [CrossRef]
169. Ama, O.M.; Kumar, N.; Adams, F.V.; Ray, S.S. Efficient and cost-effective photoelectrochemical degradation of dyes in wastewater over an exfoliated graphite-MoO_3 nanocomposite electrode. *Electrocatalysis* **2018**, *9*, 623–631. [CrossRef]
170. Qi, F.; Yang, B.; Wang, Y.; Mao, R.; Zhao, X. H_2O_2 assisted photoelectrocatalytic oxidation of Ag-cyanide complexes at metal-free g-C_3N_4 photoanode with simultaneous Ag recovery. *ACS Sustain. Chem. Eng.* **2017**, *5*, 5001–5007. [CrossRef]
171. Fan, Z.; Shi, H.; Zhao, H.; Cai, J.; Zhao, G. Application of carbon aerogel electrosorption for enhanced Bi_2WO_6 photoelectrocatalysis and elimination of trace nonylphenol. *Carbon* **2018**, *126*, 279–288. [CrossRef]
172. Zhao, X.; Zhang, J.; Qiao, M.; Liu, H.; Qu, J. Enhanced photoelectrocatalytic decomposition of copper cyanide complexes and simultaneous recovery of copper with Bi_2MoO_6 electrode under visible light by EDTA/$K_4P_2O_7$. *Environ. Sci. Technol.* **2015**, *49*, 4567–4574. [CrossRef] [PubMed]
173. Zhao, X.; Qu, J.; Liu, H.; Qiang, Z.; Liu, R.; Hu, C. Photoelectrochemical degradation of anti-inflammatory pharmaceuticals at Bi_2MoO_6-boron-doped diamond hybrid electrode under visible light irradiation. *Appl. Catal. B Environ.* **2009**, *91*, 539–545. [CrossRef]
174. Li, Y.; Chen, F.; He, R.; Wang, Y.; Tang, N. Semiconductor photocatalysis for water purification. Chapter 24. In *Nanoscale Materials in Water Purification*; Thomas, S., Pasquini, D., Leu, S.-Y., Gopakumar, D.A., Eds.; Elsevier: Amsterdam, The Netherlands, 2019; pp. 689–705.
175. Wang, Y.; Sun, J.; Li, J.; Zhao, X. Electrospinning preparation of nanostructured g-C_3N_4/$BiVO_4$ composite films with an enhanced photoelectrochemical performance. *Langmuir* **2017**, *33*, 4694–4701. [CrossRef]
176. Wang, H.; Zhang, L.; Chen, Z.; Hu, J.; Li, S.; Wang, Z.; Liu, J.; Wang, X. Semiconductor heterojunction photocatalysts: Design, construction, and photocatalytic performances. *Chem. Soc. Rev.* **2014**, *43*, 5234–5244. [CrossRef]
177. Ge, J.; Zhang, Y.; Heo, Y.-J.; Park, S.-J. Advanced design and synthesis of composite photocatalysts for the remediation of wastewater: A review. *Catalysts* **2019**, *9*, 122. [CrossRef]
178. Low, J.; Yu, J.; Jaroniec, M.; Wageh, S.; Al-Ghamdi, A.A. Heterojunction photocatalysts. *Adv. Mater.* **2017**, *29*, 1601694. [CrossRef]
179. Roul, B.; Kumar, M.; Rajpalke, M.K.; Bhat, T.N.; Krupanidhi, S.B. Binary group III-nitride based heterostructures: Band offsets and transport properties. *J. Phys. D Appl. Phys.* **2015**, *48*, 423001. [CrossRef]
180. Song, S.H.; Aydil, E.S.; Campbell, S.A. Metal-oxide broken-gap tunnel junction for copper indium gallium diselenide tandem solar cells. *Sol. Energy Mater. Sol. Cells* **2015**, *133*, 133–142. [CrossRef]
181. Guaraldo, T.T.; Goncales, V.R.; Silva, B.F.; de Toressi, S.I.C.; Zanoni, M.V.B. Hydrogen production and simultaneous photoelectrocataytic pollutant oxidation using a TiO_2/WO_3 nanostructured photoanode under visible light irradiation. *J. Electroanal. Chem.* **2016**, *765*, 188–196. [CrossRef]
182. Feleke, Z.; van de Krol, R.; Appel, P.W. Photoelectrocatalytic removal of color from water using TiO_2 and TiO_2/Cu_2O thin film electrodes under low light intensity. In *Appropriate Technologies for Environmental Protection in the Developing World*; Selected papers from ERTEP 2007, 17–19 July 2007, Ghana, Africa; Yanful, E.K., Ed.; Springer Science: Berlin/Heidelberg, Germany, 2009; pp. 181–196.

183. Liu, Z.; Wang, Q.; Rong, W.; Jin, R.; Cui, Y.; Gao, S. CTAB assisted hydrothermal preparation of Bi_2WO_6-WO_3 nanosheets on TiO_2 nanotube arrays for photoelectrocatalytic applications. *Sep. Purif. Technol.* **2018**, *200*, 191–197. [CrossRef]
184. Zhao, Q.; Wang, Q.; Liu, Z.; Qiu, L.; Tian, X.; Zhang, S. Fabrication and photoelectrochemical performance of Ag/AgBr sensitized TiO_2 nanotube arrays for environmental and energy applications. *Sep. Purif. Technol.* **2019**, *209*, 782–788. [CrossRef]
185. Fan, J.; Shi, H.; Xiao, H.; Zhao, G. Double-layer 3D macro-mesoporous metal oxide modified boron-doped diamond with enhanced photoelectrochemical performance. *ACS Appl. Mater. Interfaces* **2016**, *8*, 28306–28315. [CrossRef]
186. Rao, A.N.S.; Venkatarangaiah, V.T. Preparation, characterization, and application of Ti/TiO_2-NTs/Sb-SnO_2 electrode in photo-electrochemical treatment of industrial effluents under mild conditions. *Environ. Sci. Pollut. Res.* **2018**, *25*, 11480–11492.
187. Chen, L.-C.; Ho, Y.-C.; Guo, W.-S.; Huang, C.-M.; Pan, T.-C. Enhanced visible light-induced photoelectrocatalytic degradation of phenol by carbon nanotube-doped TiO_2 electrodes. *Electrochim. Acta* **2009**, *54*, 3884–3891. [CrossRef]
188. Hunge, Y.M.; Yadav, A.A.; Mohite, B.M.; Mathe, V.L.; Bhosale, C.H. Photoelectrocatalytic degradation of sugarcane factory wastewater using WO_3/ZnO thin films. *J. Mater. Sci. Mater. Electron.* **2018**, *29*, 3808–3816. [CrossRef]
189. Chang, K.-L.; Sun, Q.; Peng, Y.-P.; Lai, S.-W.; Sung, M.; Huang, C.-Y.; Kuo, H.-W.; Sun, J.; Lin, Y.-C. Cu_2O loaded titanate nanotube arrays for simultaneously photoelectrochemical ibuprofen oxidation and hydrogen generation. *Chemosphere* **2016**, *150*, 605–614. [CrossRef]
190. Huda, A.; Suman, P.H.; Torquato, L.D.M.; Silva, B.F.; Handoko, C.T.; Gulo, F. Visible light-driven photoelectrocatalytic degradation of acid yellow 17 using Sn_3O_4 flower-like thin films supported on Ti substrate (Sn_3O_4/TiO_2/Ti). *J. Photochem. Photobiol. A* **2019**, *376*, 196–205. [CrossRef]
191. Xu, H.; Zhang, Q.; Yan, W.; Chu, W.; Zhang, L. Preparation and characterization of PbO_2 electrodes doped with TiO_2 and its degradation effect on azo dye wastewater. *Int. J. Electrochem. Sci.* **2013**, *8*, 5382–5395.
192. Ghasemian, S.; Omanovic, S. Fabrication and characterization of photoelectrochemically-active Sb-doped Sn_x-$W_{(100-x)\%}$-oxide anodes: Towards the removal of organic pollutants from wastewater. *Appl. Surf. Sci.* **2017**, *416*, 318–328. [CrossRef]
193. Chai, S.; Zhao, G.; Li, P.; Lei, Y.; Zhang, Y.; Li, D. Novel sieve-like SnO_2/TiO_2 nanotubes with integrated photoelectrocatalysis: Fabrication and application for efficient toxicity elimination of nitrophenol wastewater. *J. Phys. Chem. C* **2011**, *115*, 18261–18269. [CrossRef]
194. Liu, D.; Zheng, Z.; Wang, C.; Yin, Y.; Liu, S.; Yang, B.; Jiang, Z. CdTe quantum encapsulated ZnO nanorods for highly efficient photoelectrochemical degradation of phenols. *J. Phys. Chem. C* **2013**, *117*, 26529–26537. [CrossRef]
195. Dawei, J.; Tianshu, Z.; Qi, S.; Yanyan, Y.; Guoyue, S.; Litong, J. Enhanced visible-light-induced photoelectrocatalytic degradation of methyl orange by CdS sensitized TiO_2 nanotube arrays electrode. *Chin. J. Chem.* **2011**, *29*, 2505–2510.
196. Wang, W.; Li, F.; Zhang, D.; Leung, D.Y.C.; Li, G. Photoelectrocatalytic degradation of organic pollutant via CdSe/TiO_2 nanotube arrays. *Appl. Surf. Sci.* **2016**, *362*, 490–497. [CrossRef]
197. Wang, X.; Wu, Q.; Ma, H.; Ma, C.; Yu, Z.; Fu, Y.; Dong, X. Fabrication of PbO_2 tipped Co_3O_4 nanowires for efficient photoelectrochemical decolorization of dye (reactive brilliant blue KN-R) wastewater. *Sol. Energy Mater. Sol. Cells* **2019**, *191*, 381–388. [CrossRef]
198. Cao, D.; Wang, Y.; Qiao, M.; Zhao, X. Enhanced photoelectrocatalytic degradation of norfloxacin by an Ag_3PO_4/$BiVO_4$ electrode with low bias. *J. Catal.* **2018**, *360*, 240–249. [CrossRef]
199. Wang, D.; Li, Y.; Puma, G.L.; Wang, C.; Wang, P.; Zhang, W.; Wang, Q. Dye sensitized photoelectrochemical cell on plasmonic Ag/AgCl @ chiral TiO_2 nanofibers for treatment of urban wastewater effluents, with simultaneous production of hydrogen and electricity. *Appl. Catal. B Environ.* **2015**, *168–169*, 25–32.
200. Rajni, K.S.; Raguram, T. Doped semiconductor as photoanode. Chapter 7. In *Interfacial Engineering in Functional Materials for Dye Sensitized Solar Cells*; Pandikumar, A., Jothivenkatachalam, K., Bhojanaa, K., Eds.; Jonh Wiley & Sons, Inc.: Hoboken, NJ, USA, 2020; pp. 139–162.
201. Zhang, H.; Li, X.; Chen, G. Fabrication of photoelectrode materials. Chapter 18. In *Electrochemistry for the Environment*; Comninellis, C., Chen, G., Eds.; Springer: Berlin/Heidelberg, Germany, 2010; pp. 473–513.

202. Almeida, L.C.; Zanoni, M.V.B. Decoration of Ti/TiO_2 nanotubes with Pt nanoparticles for enhanced UV-Vis light absorption in photoelectrocatalytic process. *J. Braz. Chem. Soc.* **2014**, *25*, 579–588.
203. He, C.; Asi, M.A.; Xiong, Y.; Shu, D.; Li, X. Photoelectrocatalytic degradation of organic pollutants in aqueous solution using a Pt-TiO_2 film. *Int. J. Photoenergy* **2009**, *634369*, 7.
204. Liu, H.; Zhong, L.; Govindaraju, S.; Yun, K. ZnO rod decorated with Ag nanoparticle for enhanced photocatalytic degradation of methylene blue. *J. Phys. Chem. Solids* **2019**, *129*, 46–53. [CrossRef]
205. Chen, Y.; Tse, W.H.; Chen, L.; Zhang, J. Ag nanoparticles-decorated ZnO nanorod array on a mechanical flexible substrate with enhanced optical and antimicrobial properties. *Nanoscale Res. Lett.* **2015**, *10*, 106. [CrossRef]
206. Gonzalez-Rodrigez, J.; Fernandez, L.; Bava, Y.B.; Buceta, D.; Vazquez-Vazquez, C.; Lopez-Quintela, M.A.; Feijoo, G.; Moreira, M.T. Enhanced photocatalytic activity of semiconductor nanocomposites doped with Ag nanoclusters under UV and visible light. *Catalysts* **2020**, *10*, 31. [CrossRef]
207. Liao, W.; Yang, J.; Zhou, H.; Murugananthan, M.; Zhang, Y. Electrochemically self-doped TiO_2 nanotube arrays for efficient visible light photoelectrocatalytic degradation of contaminants. *Electrochim. Acta* **2014**, *136*, 310–317. [CrossRef]
208. Daghrir, R.; Drogui, P.; Delegan, N.; El Khakani, M.A. Electrochemical degradation of chlortetracycline using N-doped Ti/TiO_2 photoanode under sunlight irradiations. *Water. Res.* **2013**, *47*, 6801–6810. [CrossRef]
209. Ayoubi-Feiz, B.; Mashhadizadeh, M.H.; Sheydaei, M. Preparation of reusable nano N-TiO_2/graphene/titanium grid sheet of a pesticide: Effect of parameters and neural network modelling. *J. Electroanal. Chem.* **2018**, *823*, 713–722. [CrossRef]
210. Hou, X.; Liu, X.; Han, J.; Liu, H.; Yao, J.; Li, D.; Wang, L.; Liao, B.; Li, J.; Zhang, R. Enhanced photoelectrocatalytic degradation of organic pollutants using TiO_2 nanotubes implanted with nitrogen ions. *J. Mater. Sci.* **2020**, *55*, 5843–5860. [CrossRef]
211. Zhang, G.; Miao, H.; Hu, X.; Mu, J.; Liu, X.; Han, T.; Fan, J.; Liu, E.; Yin, Y.; Wan, J. A facile strategy to fabricate Au/TiO_2 nanotubes photoelectrode with excellent photoelectrocatalytic properties. *Appl. Surf. Sci.* **2017**, *391*, 345–352. [CrossRef]
212. Cheng, X.; Liu, H.; Chen, Q.; Li, J.; Wang, P. Construction of N, S codoped TiO_2 NCs decorated TiO_2 nano-tube array photoelectrode and its enhanced visible light photocatalytic mechanism. *Electrochim. Acta* **2013**, *103*, 134–142. [CrossRef]
213. Peng, Y.-P.; Chen, H.; Huang, C.P. The synergistic effect of photoelectrochemical (PEC) reactions exemplified by concurrent perfluorooctanoic acid (PFOA) degradation and hydrogen generation over carbon and nitrogen codoped TiO_2 nanotube arrays (C-N-TNTAs) photoelectrode. *Appl. Catal. B Environ.* **2017**, *209*, 437–446. [CrossRef]
214. Zhou, X.; Zhang, X.; Feng, X.; Zhou, J.; Zhou, S. Preparation of a La/N co-doped TiO_2 film electrode with visible light response and its photoelectrocatalytic activity on a Ni substrate. *Dyes Pigm.* **2016**, *125*, 375–383. [CrossRef]
215. Bessegato, G.G.; Cardoso, J.C.; Zanoni, M.V.B. Enhanced photoelectrocatalytic degradation of an acid dye with boron-doped TiO_2 nanotube anodes. *Catal. Today* **2015**, *240*, 100–106. [CrossRef]
216. Chen, Q.; Liu, H.; Xin, Y.; Cheng, X. Coupling immobilized TiO_2 nanobelts and Au nanoparticles for enhanced photocatalytic and photoelectrocatalytic activity and mechanism insights. *Chem. Eng. J.* **2014**, *141*, 145–154. [CrossRef]
217. Wang, Q.; Wang, X.; Zhang, M.; Li, G.; Gao, S.; Li, M.; Zhang, Y. Influence of Ag-Au microstructure on the photoelectrocatalytic performance of TiO_2 nanotube array photocatalysts. *J. Colloid Interface Sci.* **2016**, *463*, 308–316. [CrossRef]
218. Zhong, J.S.; Wang, Q.Y.; Zhou, J.; Chen, D.Q.; Ji, Z.G. Highly efficient photoelectrocatalytic removal of RhB and Cr(VI) by Cu nanoparticles sensitized TiO_2 nanotube arrays. *Appl. Surf. Sci.* **2016**, *317*, 342–346. [CrossRef]
219. Zhou, K.; Tian, Y.; Ma, C.; Fu, Y.; Dong, X.; Zhang, X. Photoelectrocatalytic performance of conductive carbon black-modified Ti/F-PbO_2 anode for degradation of dye wastewater (reactive brilliant blue KN-R). *J. Solid State Electrochem.* **2018**, *22*, 1131–1141. [CrossRef]
220. Goulart, L.A.; Alves, S.A.; Mascaro, L.H. Photoelectrochemical degradation of bisphenol A using Cu doped WO_3 electrodes. *J. Electroanal. Chem.* **2019**, *39*, 123–133. [CrossRef]

221. Zhang, Y.; Yi, Z.; Wu, G.; Shen, Q. Novel Y doped $BiVO_4$ thin film electrodes for enhanced photoelectric and photocatalytic performance. *J. Photochem. Photobiol. A* **2016**, *327*, 25–32. [CrossRef]
222. Liao, P.; Carter, E.A. New concepts and modelling strategies to design and evaluate photo-electro-catalysts based on transition metal oxides. *Chem. Soc. Rev.* **2013**, *42*, 2401–2422. [CrossRef]